Response_to_Reviewers .pdf

Multi_Period_ULF_Modulation_BD_IES_Observation_TRACK_CHANGE.pdf

Response to Reviewer

We would like to thank both reviewers for carefully reading our manuscript and providing constructive comments. We appreciate that the reviewers introduce recent progress on related topics. We particularly notice the issue concerning the derivation of Equations 5-8 in our manuscript, which could indeed be critical to the scientific content. We have examined every equations in the manuscript.

In the following, we first clarify the derivation of equation 5-8 in our manuscript. Then, we provide a one-on-one response to the reviewers' comments.

1. Derivation of Equations 5-8 in the manuscript

The drift-resonance theory developed by Southwood and Kivelson was basically an integral of the particle energy change along the unperturbed particle drift trajectory (in a dipole background magnetic field). This unperturbed particle orbit integration method is the most common, straightforward method used in studies of ULF wave-particle interaction.

Here, starting with the wave electric field in the original Southwood and Kivelson theory, we demonstrate how different terms were introduced into the theory to obtain a modeled wave electric field described by Equation 8 in the manuscript. We show that the wave electric field given by Equation 8 corresponds to the magnetic vector potential given by Equations 5-7. We hope that our clarification can address the review's concern.

The wave electric field was originally given in the simplest form by:

$$\vec{E} = E_\varphi \hat{e}_\varphi \tag{Eq. 1}$$

and

$$E_\varphi = E_0 \exp[i(m\varphi - \omega t)] \tag{Eq. 2}$$

which describes an oscillation of constant amplitude E_0 at the angular frequency ω.

Zhou et al., 2005 & 2006 introduce the term $\exp\left[-\frac{t^2}{\tau^2}\right]$ to describe the growth and damping of the wave amplitude. The wave electric field now becomes:

$$E_\varphi = E_0 \exp\left[-\frac{t^2}{\tau^2}\right] \exp[i(m\varphi - \omega t)] \tag{Eq. 3}$$

The amplitude of the wave increases from 0 at t=-∞, reaches its maximum E_0 at t=0, and decreases to 0 at t=+∞. The rate of growth and damping is described by the time scale τ. If we further allow the wave to grow at the time scale τ_+, reach its maximum amplitude at t_0, and damp at the time scale τ-, Eq. 3 rewrites as:

$$E_\varphi = E_0 \exp\left[-\frac{(t-t_0)^2}{{\tau_\pm}^2}\right] \exp[i(m\varphi - \omega t)]$$

(Eq. 4)

Li et al., 2017 introduced the term $\frac{\exp[\xi \cos(\varphi-\varphi_0)]}{2\pi I_0(\xi)}$ to describe the azimuthal localization of the wave. The figure below illustrates the value of $f_{VM} = \frac{\exp[\xi \cos(\varphi-\varphi_0)]}{2\pi I_0(\xi)}$ for different concentration parameter ξ, where the x-Axis denotes $\phi=\varphi-\varphi_0$.

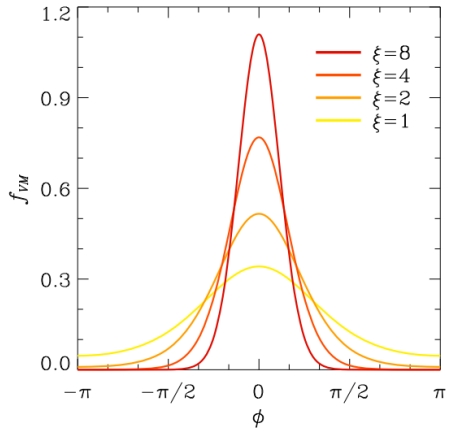

With the distribution of the wave amplitude in the azimuthal direction described by $\frac{\exp[\xi \cos(\varphi-\varphi_0)]}{2\pi I_0(\xi)}$, the wave electric field becomes:

$$E_\varphi = E_0 \frac{\exp[\xi \cos(\varphi-\varphi_0)]}{2\pi I_0(\xi)} \exp\left[-\frac{(t-t_0)^2}{{\tau_\pm}^2}\right] \exp[i(m\varphi - \omega t)]$$

(Eq. 5)

The amplitude of the wave electric field also depends on radial distance to the Earth's center. We use a general term G(r) to describe the radial dependence:

$$E_\varphi = E_0 \mathrm{G(r)} \frac{\exp[\xi \cos(\varphi-\varphi_0)]}{2\pi I_0(\xi)} \exp\left[-\frac{(t-t_0)^2}{{\tau_\pm}^2}\right] \exp[i(m\varphi - \omega t)]$$

(Eq. 6)

Since we are dealing with two monochromatic wave in our manuscript, we allow each of the monochromatic wave to have its own initial phase, by adding θ_0 in the oscillation term $\exp[i(m\varphi - \omega t)]$. Also, for the consistency of the variable names, the constant factor E_0 is replaced by A_0. Now we obtain the wave electric field of each monochromatic ULF wave in the form shown in Equation 8 in our manuscript:

$$E_\varphi = A_0 \mathrm{G(r)} \frac{\exp[\xi \cos(\varphi - \varphi_0)]}{2\pi I_0(\xi)} \exp\left[-\frac{(t-t_0)^2}{{\tau_\pm}^2}\right] \exp[i(m\varphi - \omega t + \theta)]$$

(Eq. 7)

Then, we will demonstrate that such wave electric field corresponds to magnetic vector potential described by Equations 5-7 in our manuscript.

Since $\nabla \times \vec{E} = -\frac{\partial \vec{B}}{\partial t} = -\frac{\partial(\nabla \times \vec{A})}{\partial t} = \nabla \times \left(-\frac{\partial \vec{A}}{\partial t}\right)$, a magnetic vector potential defined by $\vec{A} = \int_{-\infty}^{t} \vec{E} dt$ guarantee that the corresponding $\vec{E}$ and $\vec{B} = \nabla \times \vec{A}$ follows the Faraday's law.

In a general form, the integral $\int_{-\infty}^{t} \exp\left[-\frac{(x-A)^2}{B^2}\right] \exp[i(C - Dx)] dx$ yields:

$$\int_{-\infty}^{t} \exp\left[-\frac{(x-A)^2}{B^2}\right] \exp[i(C - Dx)] dx$$
$$= \frac{\sqrt{\pi}}{2} B \exp\left[-\frac{1}{4}B^2D^2 + (C - AD)i\right] \left(\mathrm{erf}\left[-\frac{t-A}{B} + \frac{BD}{2}i\right] + 1\right)$$

(Eq. 8)

where A, B, C, and D are parameters independent of variable x.

From Eq. 8, it is easy to obtain:

$$\int_{t_0}^{t} \exp\left[-\frac{(x-A)^2}{B^2}\right] \exp[i(C - Dx)] dx$$
$$= \frac{\sqrt{\pi}}{2} B \exp\left[-\frac{B^2D^2}{4}\right] \left(\mathrm{erf}\left[-\frac{t-A}{B} + \frac{BD}{2}i\right] - \mathrm{erf}\left[-\frac{t_0-A}{B} + \frac{BD}{2}i\right]\right) \exp[i(C - AD)]$$

(Eq. 9)

Let A=t_0, B=τ, C=mφ+θ_0, and D=ω, using Equations 8 and 9, we have:

$$\int_{t_0}^{t} \exp\left[-\frac{(t-t_0)^2}{{\tau_\pm}^2}\right] \exp[i(m\varphi - \omega t + \theta_0)] dt$$
$$= \frac{\sqrt{\pi}}{2} \tau_\pm \exp\left[-\frac{{\tau_\pm}^2\omega^2}{4}\right] \cdot \left(\mathrm{erf}\left[-\frac{t-t_0}{\tau_\pm} + \frac{\tau_\pm \omega}{2}i\right] - \mathrm{erf}\left[\frac{\tau_\pm \omega}{2}i\right]\right) \exp[i(m\varphi - \omega t_0 + \theta_0)]$$

(Eq. 10)

and

$$\int_{-\infty}^{t_0} \exp\left[-\frac{(t-t_0)^2}{{\tau_+}^2}\right] \exp[i(m\varphi - \omega t + \theta_0)] dt$$
$$= \frac{\sqrt{\pi}}{2} \tau_+ \exp\left[-\frac{{\tau_+}^2\omega^2}{4}\right] \cdot \left(\mathrm{erf}\left[\frac{\tau_+ \omega}{2}i\right] + 1\right) \exp[i(m\varphi - \omega t_0 + \theta_0)]$$

(Eq. 11)

Using Equations 10 and 11, we have:

$$\int_{-\infty}^{t_0} E_\varphi dt = \int_{-\infty}^{t} A_0 \mathrm{G(r)} \frac{\exp[\xi\cos(\varphi-\varphi_0)]}{2\pi I_0(\xi)} \exp\left[-\frac{(t-t_0)^2}{{\tau_\pm}^2}\right] \exp[i(m\varphi-\omega t+\theta)]dt$$

$$= A_0 \mathrm{G(r)} \frac{\exp[\xi\cos(\varphi-\varphi_0)]}{2\pi I_0(\xi)} \int_{-\infty}^{t} \exp\left[-\frac{(t-t_0)^2}{{\tau_\pm}^2}\right] \exp[i(m\varphi-\omega t+\theta)]dt$$

$$= A_0 \mathrm{G(r)} \frac{\exp[\xi\cos(\varphi-\varphi_0)]}{2\pi I_0(\xi)} \left(\begin{array}{l} \int_{-\infty}^{t_0} \exp\left[-\frac{(t-t_0)^2}{{\tau_+}^2}\right] \exp[i(m\varphi-\omega t+\theta_0)]dt \\ + \int_{t_0}^{t} \exp\left[-\frac{(t-t_0)^2}{{\tau_\pm}^2}\right] \exp[i(m\varphi-\omega t+\theta)]dt \end{array} \right)$$

$$= A_0 \mathrm{G(r)} \frac{\exp[\xi\cos(\varphi-\varphi_0)]}{2\pi I_0(\xi)}$$

$$\cdot \left\{ \begin{array}{l} \frac{\sqrt{\pi}}{2}\tau_+ \exp\left[-\frac{{\tau_+}^2\omega^2}{4}\right] \cdot \left(\mathrm{erf}\left[\frac{\tau_+\omega}{2}i\right]+1\right) \exp[i(m\varphi-\omega t_0+\theta_0)] \\ + \frac{\sqrt{\pi}}{2}\tau_\pm \exp\left[-\frac{{\tau_\pm}^2\omega^2}{4}\right] \cdot \left(\mathrm{erf}\left[-\frac{t-t_0}{\tau_\pm}+\frac{\tau_\pm\omega}{2}i\right]-\mathrm{erf}\left[\frac{\tau_\pm\omega}{2}i\right]\right) \exp[i(m\varphi-\omega t_0+\theta_0)] \end{array} \right\}$$

(Eq. 12)

Though the expression seems a little lengthy, the only term in the final result of Equation 12 which depends on time is shown in red.

We define F as the terms in the curly brackets in Equation 12:

$$F = \frac{\sqrt{\pi}}{2}\tau_\pm \exp\left[-\frac{{\tau_\pm}^2\omega^2}{4}\right] \cdot \mathrm{erf}\left[-\frac{t-t_0}{\tau_\pm}+\frac{\tau_\pm\omega}{2}i\right] \exp[i(m\varphi-\omega t_0+\theta_0)] + C$$

(Eq. 13)

where C is defined as the rest terms in the curly brackets in Equation 12 which are independent of time.

Using Equations 12 and 13, we define:

$$A = \int_{-\infty}^{t_0} E_\varphi dt = A_0 \mathrm{G(r)} \frac{\exp[\xi\cos(\varphi-\varphi_0)]}{2\pi I_0(\xi)} F$$

(Eq. 14)

A, F, and C defined here are identical to those in Equations 5-7 in our manuscript (for one monochromatic wave).

So far, we have demonstrated the meaning of the different terms in our wave electric field, and have proved the derivation of equations 5-8 in our manuscript. We hope that the demonstration here can clarify the equations in our manuscript.

2. One-on-One Responses

In this section, we present one-on-one responses to reviewer's comments, as well as the list of changes in the revised manuscript. (The comments of the reviewer will be shown in **blue** and our responses will be shown in **black**.)

Reviewer #1

Line 7: "We adopt the calculation scheme therein to derive the electron energy change in a multi-period ULF wave field"
Are there other kinds of schemes to explain this energy change in ULF wave field? If yes, the authors are suggested to briefly talk about at least one of them and explain why they choose the specific scheme.

We adopt the drift-resonance theory developed by Southwood and Kivelson, 1981 to explain the multi-period electron flux modulation observed by BD-IES. As described in the previous section, the theory is essentially an integral of energy change along the unperturbed particle orbit. This unperturbed orbit integration method is the most common, straightforward method, and it is sufficient to reveal the most of the underlying physics of ULF wave-particle interaction (e.g. Claudepierre et al., 2013; Dai et al., 2013; Hao et al., 2014, 2017, 2019; Li et al., 2017a, 2017b, Zhou et al., 2015, 2016; Zong et al., 2007, 2009), including the observations in the present study.
As for other schemes, Li et al., 2018 employed a pendulum equation to study the particle energy change with the perturbed orbit taken into account. Also, a number of numerical simulations were conducted to study the particle energy change in a ULF wave field (e.g. Degeling et al., 2018; Hudson et al., 2001).
We replace "scheme" by "method" here and throughout the manuscript. We also revise Section 4.4 to elaborate a bit on the perturbed particle trajectory and its non-linear effects.

Line 23: "…, called the resonance energy, at which the particles would experience a stable electric field during their drift motion, …"
What about magnetic field experienced by particles?

The particle would definitely experience a wave magnetic field. (Otherwise, it violets Faraday's law.) However, since Lorentz force is always perpendicular to particle velocity, it does no work on the particle.

Also, "stable" might not be an accurate or even a necessary word here. The unstable force could also affect particles as long as the resonance condition is met.

We agree with the reviewer that "stable" is not the proper word here. We replace it by "steady", which means that the sign of the electric field experienced by the particle does not change.

Line 39: "In addition, ULF waves in the magnetosphere have been found to be asymmetrically distributed (e.g. Takahashi et al., 1985; Liu et al., 2009), whereas a symmetric ULF wave field is assumed in the conventional drift-resonance theory."
Mentioning recent works that address the distribution of the ULF waves is suggested. For example, Barani, M., Tu, W., Sarris, T., Pham, K., & Redmon, R. J. (2019). Estimating the

azimuthal mode structure of ULF waves based on multiple GOES satellite observations. Journal of Geophysical Research: Space Physics, 124, 5009–5026. Figure 5 (a & b) as well as figures 6 of the mentioned paper and the explanations therein clearly show that the wave can be azimuthally localized. It is also suggested that for the sake of clarity authors mention which "symmetry" they are talking about; the symmetry mentioned in the Figure 2 of Southwood and Kivelson (1981) or they are generally talking about the homogeneity of ULF amplitude (power) pulsations in the azimuthal direction? If the latter is meant, bringing the word "symmetry" could be miss-leading.

We thank the reviewer for introducing recent papers on related topics. We include these recent findings in our revised introduction section (Line 40).
We agree with the reviewer that "symmetric" is not the proper word here and rephrase as "uniform" (Line 40). Besides, "asymmetric" is replaced by "azimuthally localized".

Line 63: "The electron flux data in this study are obtained by the BeiDa Imaging Electron Spectrometer (BD-IES) onboard a 55 inclined geosynchronous orbit (IGSO) spacecraft of China"
Since the study is conducted for equatorially mirroring electrons (~0 degree pitch angle), the following questions must be addressed in section 2 of the manuscript: Did the authors project (map) the data to the equatorial plane? If yes, which scheme/methods they applied. If not, how this 55-degree inclination would affect/alter the results.
Which level of the data is used? What is the spin period and the spin axis direction of the spacecraft? Is the de-spun data used for the analysis in this manuscript?

We did not project the data. We will justify the way we used the electron flux data in the response to comments on Line 112 (concerning the issue that we used omnidirectional flux but perform the numerical calculation with equatorially mirroring electron).
The spacecraft with BD-IES onboard is not a spinning spacecraft. (See Zong et al., 2018 for more information about the instrument and spacecraft)

Line 86: The residual flux, defined as $(J-J_{Avg})/J_{Avg}$, represents the flux variation normalized to the background flux so that the relative change of the particle flux caused by the waves can be quantitatively compared across different energy channels.
As the authors correctly stated later, the J_{Avg} is not necessarily $J_{background}$. So, this might be misleading to name J_{Avg} as background flux.

Agree. "$(J-J_{Avg})/J_{Avg}$" is replaced by "$(J-J_0)/J_0$" where J_0 represents the background trend of the flux.

Line 93: "… to display the wavelet power spectrum."
Some basic information about the way the authors conduct the Wavelet analysis is highly suggested and should be addressed such as: Name of the mother wavelet, the cadence of the data used as the input to the wavelet computation functions, the scale (frequency) range selected for the wavelet analysis.
The reviewer (for his reference) is interested in learning about the scale (frequency) spacing in the output of the wavelet function. (In other words, what is the y axis spacing/resolution between the data points in Figure 2 and which shading method was

used in the color-coded visualization in that figure?)

We use Morlet wavelet, with ω_0=6. The cadence of the input for the wavelet analysis is 10 seconds, the same as the cadence of the data product of BD-IES. More specifically, the only difference between the original electron flux data and the input for the wavelet analysis is that the bad data are removed by a linear interpolation of the valid data in the nearest neighbor.
The wavelet power is defined as the product of wavelet transform multiplied by its conjugate (Torrence and Compo, 1998). Therefore, given a frequency (scale), the corresponding wavelet power can be calculated. To create Figure 2, we calculated the wavelet power at 201 frequencies that corresponds to periods evenly distributed in the range from 100 sec to 500 sec. We change the opacity of the part of the figure using Adobe illustrator to obtain the shading effect.

Line 94: "As the wavelet power is proportional to the square of the oscillation amplitude … ."
Please pay attention that this is the case for any power hopefully regardless of the spectral analysis methods such as FFT, WFFT, Wavelet, … .

Agree. We specify wavelet power here, as it is the analysis method we use.

Line 100: "Besides, the electron flux modulation exhibits a dispersive characteristic."
What kind of dispersive? In other words, dispersive with respect which quantity?

We rephrase as "energy dispersive characteristic", which means the modulation was observed first at higher energy and then at lower energy.

Line 112: "For a symmetric background magnetic field, the unperturbed drift orbit of an equatorial mirroring particle can be given by … "
Here in the model the authors look at ~90-degree pitch angle (or equatorially mirroring) electrons while in the measured flux data omni-directional particles' differential flux was analyzed. How this discrepancy can be addressed? Further information/reasoning or references seems to be needed to make sense of this omni-directional choice specially for those whose primary research focus is not looking at particle flux/phase space density data.

Here, we justify our usage of the BD-IES data.
As the time scale of the problem we study (in the order of hundreds of seconds) is much longer than the bounce period of the particle (in the order of a second), we assume that any inhomogeneity would be quickly dispersed along the bounce path of the particle. Therefore, the measurement of electron flux off the equator at energy W and pitch angle α corresponds the electron flux at the equator at energy W and equatorial pitch angle α_{Eq}.
As demonstrated in the introduction section of our manuscript, the key parameter for a particle interacting with a monochromatic ULF wave via drift-resonance is its angular drift velocity ω_d. In a dipole field, ω_d is in proportion to $W(0.35+0.15\sin\alpha_{Eq})$. Therefore, the phase difference between the flux modulations is larger at different energies than at different pitch angles. Thus, we can still see pattern of flux modulation caused by drift-resonance in the omnidirectional fluxes at different energies.
e.g. Li et al., 2017a, 2017b used BD-IES data in the same way.

Line 123: "Therefore, particle flux modulation caused by drift-resonance would present a characteristic 180 phase shift across the resonant energy."
It is strongly suggested that the authors bring some key previous works observing this phenomenon.

We list a few papers observing this phenomenon in the introduction section (e.g. Line 34)

Line 129: "Then, when the wave starts damping, the phase shift would keep growing as the drift velocities of the particles depend on their energies"
Clarifying the connection between dependency of particles' drift frequency on their energy and growth of the phase shift in δW after the onset of wave damping is suggested here even by adding one/few sentences.

The connection is quantitatively described by Equation 14 in Zhou et al., 2016, elaborated in text in the paragraph following Equation 14, and illustrated in their Figure 2. The following sentence "This characteristic phase relationship is presented as increasing tilted stripes in the particle flux spectrogram" describes the characteristics of the phase shift cause by a damping wave.

Line 135: "While the characteristic particle signatures of drift-resonance predicted by these prevailing theories have been proved by recent spacecraft observations, the particle energy change therein is derived in an incomplete way"
References on recent spacecraft observations that proved the mentioned drift-resonance driven behavior of particles flux should be added.

As this comment is related to the comments on Line 39, please see our replies there.

Line 140: "The Betatron acceleration caused by the curl of the wave electric field, denoted by $\mu/\gamma \partial B/\partial t$ is omitted in those drift-resonance theories.
Again, referring to some of the main papers (in addition to Southwood and Kivelson (1981)) on those theories is needed.

Zhou et al., 2015, 2016, Li et al.,2017b mentioned in the previous paragraph (Line 125-134) are all among papers of "those theories".

Line 141: "One might neglect this energy change, because the magnetic field of fundamental mode waves has a node at the equator. Especially in the case of a purely poloidal wave, the perpendicular component of the wave magnetic field B_r can be identically zero in the equatorial plane"

We would like to clarify first that E_φ, B_r, and B_z give the poloidal mode wave; E_r and B_φ give the toroidal wave. To describe a poloidal wave, one can first define B_r and B_z, then derives E_φ according to Faraday's law. Alternatively, one can first define E_φ, then use Faraday's law to derive B_r and B_z.

The reviewer's immediate understanding is that this reasoning might not be necessarily valid for all ULF wave cases. For example, for broadband ULF pulsations which is different from the field line resonance oscillations we do not necessarily have a node in the equatorial plane.

By saying "can be zero", we mean that it is possible to be zero, not that it is always zero. Nevertheless, we remove these two sentences, since they possibly lead to misunderstandings.

Looking at equation $dW/dt = q\boldsymbol{E}\cdot\boldsymbol{u} + \mu/\gamma \partial B/\partial t$, we can see that vanishing/small B_r has no effect on making the $\partial B/\partial t$ term zero. Since it is the change of B in time that determines the second term, not the B itself. If the authors meant $\partial B_r/\partial t$ (not B_r itself) in the text, the explanation/reasoning should be provided since in the fundamental mode (Figure 2 panel (a) in Southwood and Kivelson (1981)) the temporal change of B in the equatorial plane is actually maximum.

$\partial B/\partial t$, as it appears here, means $\partial B/\partial t$, not $\partial B_r/\partial t$ guessed by the reviewer.
In the paragraph from Lines 135-153, we are arguing that $\partial B/\partial t$ can not be neglected in the general case. After the sentence in Line 141 quoted by the reviewer, we immediately state in the next sentence that the neglect of this energy change is not correct.

Line 143: "However, even then, there would still be a non-negligible change of magnetic field magnitude, because there should be a parallel wave magnetic field B_z according to [the] Faraday's law." Correct, although we do not have to assume that there is always an E_φ. Since $\partial E_r/\partial \varphi$ can also give non-zero B_z.

Since we focus on poloidal wave, we study E_φ, B_r, and B_z, though E_φ in an actual case can be zero.

Line 146: "Note that, for poloidal waves, $\nabla \times E$ is controlled by $\partial E/\partial r$ since E is in the azimuthal direction. Consequently, the particle energy change would be greatly influenced by the radial gradient of wave electric field amplitude, although the particle drifts at a constant L shell in the unperturbed orbit approximation."
If the reviewer understood correctly, poloidal component for dipole field at equatorial plane means Br, and following Faraday's law, $\partial B_r/\partial t = -(\nabla \times E)_r = -1/r \partial E_z/\partial \varphi + r\partial E_\varphi/\partial z$. Therefore, the reviewer does not see the effect of $\partial E/\partial r$ for poloidal component of pulsations, and more explanation by the authors is necessary here.
Also, the readers should notice that only in a pure dipole field, the poloidal means B_r at equatorial plane. However, in the more general case of non-dipole or extension of the study to non-zero magnetic latitudes, it does not have to only be B_r.

The poloidal wave has components of E_φ, B_r, and B_z. Following Faraday's law,
$\partial B_r/\partial t = -(\nabla \times E)_r = -1/r \partial E_z/\partial \varphi + \partial E_\varphi/\partial z = \partial E_\varphi/\partial z$

$\partial B_z/\partial t = -(\nabla \times E)_z = -1/r \partial(rE_\varphi)/\partial r + 1/r \partial E_r/\partial \varphi = -1/r \partial(rE_\varphi)/\partial r$

Therefore, $\partial E_\varphi/\partial r$ affects B_z.

Line 153: "The background field is given by $B_0 = \cdots = B_E/r^3 e_z$ where …"
In the denominator, there should be L instead of r. It is suggested the authors review all of the derivations and make sure that this typo/mistake was not present in their calculations.

Agree. "r" here should be replaced by "r/R_E" which is identical to "L".

Line 157: "The poloidal ULF wave fields can be given in a general form by $\boldsymbol{E}_1 =$

$-\partial A/\partial t e_\varphi \triangleq$ …"

It is worth noticing that in a general case there is an electric potential term. So, the general form for an electric field can be $\boldsymbol{E}_1 = -\boldsymbol{\nabla}\phi - \partial \boldsymbol{A}/\partial t$. Therefore, it would be very useful if the authors could shortly talk (or bring references) about why $-\nabla\phi$ is neglected here and how likely the electrons face a free electric potential field in the magnetosphere during their drift around Earth.

We agree with the reviewer that "general form" might not be the proper word here.
As we demonstrated in the previous section, the wave electric field in Southwood and Kivelson type theories of drift-resonance is defined somewhat arbitrarily. In such cases, the wave magnetic field can not be arbitrarily defined. For a given wave electric field, we can solve the equation $\mathbf{E}=-\partial\mathbf{A}/\partial t$ to obtain A, and then define the wave magnetic field as $\mathbf{B}=\boldsymbol{\nabla}\times\mathbf{A}$. This scheme is general in the sense that it is not restricted to a specific form of the wave electric field. Nevertheless, "general" is not a proper word here. We remove "in a general form" in the revised manuscript. (Line 157)

Line 158: "For fundamental mode waves, it is reasonable to further assume that the amplitude of the wave does not vary in the vicinity of equator (i.e. $\partial \boldsymbol{A}/\partial z = 0$)"
Please look at the reviewer's comment under Line 141.

Our response is also presented above.

Line 162:
Relation (4) in the manuscript is neat. It is very good that the authors quantitatively explain the correction while considering a more general case although yet limited to the odd (and probably not even) modes of field line resonances.

We agree that Relation 4 may not apply to even modes.

Line 184 Equation (6):
In the exponential, there we see $t_{0,n}$ while it cannot be a constant. Having a constant time in the exponential means F_n would not give a wave behavior. The reviewer's understanding is that it should be t instead. Otherwise, authors are required to explain how the wave behavior is represented in the mentioned equation.

As we demonstrated in the previous section. The derivation of Equation 6 in the manuscript is correct. The term that varies with time is $\mathrm{erf}\left[-\frac{t-t_0}{\tau_\pm}+\frac{\tau_\pm\omega}{2}i\right]$. The error function erf(z) is a monotonically increasing function when the argument z is a real number. However, when the argument is a complex number, the error function can give a wave behavior. (See e.g. https://mathworld.wolfram.com/Erf.html for reference)

Line 190 Right hand side of Equation (8):
If we take time derivative of $\boldsymbol{A}$, we will get two terms: one is exactly what we see in Equation (8), another is proportional to $i\omega_n$ multiplied by the error function. Explanation of why we should not get the second term (or if we get, why that term must be neglected) is necessary here.
The reviewer stops here and would let the authors provide their reasonings, explanations,

and corrections since the final results and conclusion might depend on these corrections

Related to the comments on Line 184 Equation 6, the term $\exp\left[i\left(m_n\varphi - \omega_n t_{0,n} + \theta_{0,n}\right)\right]$ is correct in the form it appears. $t_{0,n}$ should not be replaced by t. Therefore, the "second term" does not exist.

Comments on Figures

Figure 1:
What are the narrow white-color vertical lines in the spectrogram (a) panel?
The reviewer suggests bringing the MLT and MLAT information to the readers' attention as captions under panel (d) or by briefly addressing them in the text. There, no information of the solar wind (such as solar wind P_{dyn}, IMF Bz, as well as geomagnetic Dst, and AE) is given, and the readers would not be able to track any relation between the plots and the geomagnetic and solar wind indices. Following or not following the mentioned suggestions here is not critical and would not affect the reviewer's final decision.

We agree with the reviewer that information about the spacecraft position should be provided. Spacecraft position is provided in the revised figure.
Since we focus on the wave-particle interaction (instead of issues such as the excitation of the wave or the source of the particle), the solar wind, IMF condition, and the geomagnetic index may not be crucial here.

White color in Fig 1a refers to "no valid data". For example, the instrument recorded bad data at UT~10:32. In panels c and d, the bad data appear as breakpoints in the time series of the electron flux. Accordingly, there is a white line in panel a.

Figure 2 and line 82:
Is the dimension of the plots amplitude squared, or amplitude squared over frequency? If it is just the power (former case), there should be an explanation on how the power is deduced (i.e. is it an averaged value or summed over scale (frequency) range from … to …) since typically the spectral analysis codes give the analysis in terms of power density not power.

Figure 2 shows the wavelet power, defined as the product of wavelet transform multiplied by its conjugate (See Torrence and Compo, 1998 for reference)

Minor comments

Line 11: "wave electron field"
It should be wave electric field.

Agree. The typo is corrected.

Line 52: "First, we revisit the origin drift-resonance theory…"
Do the authors mean the origin of the or they mean original?

"Origin" is corrected by "original".

Line 54: "We show that the Betatron acceleration caused by the curl of the wave electric field, which is omitted in these theories, is comparable with the energy change caused by

the poloidal electric field along the drift trajectory of the particle"
Before Betatron acceleration there should be energy change due to.

If "Betatron acceleration" refers to the acceleration process, "energy change due to" should be added. If "Betatron acceleration" refers to the result that particle are accelerated by the Betatron acceleration process, "energy change due to" might not be added.

Line 72: "The IGSO spacecraft with BDIES onboard passes through the radiation belt twice per orbit. Figures 1a and 1b show the electron flux in a full pass of the spacecraft through the radiation belt in the format of spectrogram and series plot respectively."
It is suggested that before the words radiation belt there should be outer.
plot should be plots
In the spectrogram, did you use any kind of interpolation or smoothing?

Agree. It should be outer radiation belt. "plot" should be "plots".
No interpolation or smoothing is used in the spectrogram

Line 95: "…, the upper limit of the colorbar for each energy channel is chosen to be the square of the mean value of the electron flux in the selected interval from 10:15 UT to 11:15 UT and the widths of the colorbars are consistently set to be 2."
Which Figure the manuscript is pointing to? Dimension of the value should be mentioned: for example, is it power or power over frequency?
Did you detrend the signals? If yes, what was the detrending method and width of the moving average scheme?

"colorbar" in Line 95 refers to Figure 2 as we are discussing the wavelet power in the context.
Figure 2 shows the wavelet power, defined as the product of wavelet transform multiplied by its conjugate (See Torrence and Compo, 1998 for reference).
No detrending is applied to the data before wavelet analysis. As we demonstrate in Line 93, we use the choice of colorbars to achieve comparison across energy channels instead of detrending the data.

Line 112:"For a symmetric background magnetic field, the unperturbed drift orbit of an equatorial mirroring particle can be given by … "
It should be equatorially mirroring particles.

Agree. "equatorial mirroring particle" is not grammatically correct. It should be "equatorially mirroring particle"

Line 143: "However, even then, there would still be a non-negligible change of magnetic field magnitude, because there should be a parallel wave magnetic field B_z according to the Faraday's law."
the should be deleted.

Agree. The redundant "the" is deleted

Line 165: redundant the

Agree. The redundant "the" is deleted

Line 165: "For the empirical electric field model denoted by $E_\varphi \propto \exp[\sigma r]$ (e.g. Perry et al., 2005; Ozeke et al., 2014), …"
Which paragraph or equation number in the aforementioned references the authors are specifically pointing to?
As σ is set to be a positive value, the authors should bring a proper reference or explanation on the limitation of the exponential behavior with positive power in E_φ.

Equation 19 in Perry et al., 2005; Equation 10 in Ozeke et al., 2014.
Perry et al., 2005, for example, used the exponential term to describe the wave amplitude from L~2 to L~9.

Line 171: "According to Li et al. (2017b), this dispersive characteristic implies that the ULF waves were azimuthally confined…"
Again, referring to a direct measure/evidence of this azimuthally confined ULF waves power (such as Barani et al. (2019)) would strengthen the authors' argument on the validity of defining an envelope in the azimuthal direction.

The direct evidence of azimuthally confined ULF waves is included in the introduction section. By referring to Li et al., (2017b) here, we want to demonstrate that such particle characteristic (also observed in the present study) can be explained by azimuthally localized wave.

Line 178: "The constant factor $A_{0,}$ denotes the amplitude of the wave. The second term (r) describe of wave amplitude in the radial direction"
If defining two different amplitudes for a wave is not common, the reviewer suggests using a different language for the sake of clarity avoiding two-amplitude language.
We avoid wording such as "two-amplitude of one wave". We rephrase as "For each monochromatic wave, we define its amplitude as $A_{0,n}$."
describe of should be describes
Agree. Corrected.

Line 178: "The third term $(\varphi) =$… is a von Mises function, …"
As H_n here is not just function of n and φ, it would be more inclusive/accurate to use the notation $H_n(\varphi|\varphi_0, \xi_n)$ instead of $H_n(\varphi)$.

Agree. While φ is the variable, $\varphi_{0,n}$ and ξ_n are constant parameters that affect the value of the function H. Note that ω, τ, t_0, and θ_0 are all parameters that affect the value of F. As it may be too lengthy to list all the parameters, we only show the variable(s) in the bracket,

Line 182: "…is the zeroth-order modified Bessel function."
It should be modified Bessel function of the first kind.

Agree. Corrected.

Line 182: "The von Mises distribution is an analogue of the normal distribution."
The reviewer suggests adding words like in the rotational/periodic scheme at the end of this sentence.

Agree. "for a periodic variable" is added.

Reviewer #2

Line 227, 'they corresponds to' –> they correspond to
Line 286, 'with a azimuthally' –> with an azimuthally
Line 287, 'between the our' –> between our
Line 292, 'the azimuthal concentration of the waves extend' –> the azimuthal concentration of the waves extends

Thanks for pointing out the typos. They are corrected accordingly in the revised manuscript.

Line 299, the link of BD-IES is not accessible. Please check this.

We notice that the link of BD-IES provided in Line 299 no longer works. The new access to the data can be found at http://beidou.gov.cn/yw/gfgg/201912/t20191209_19614.html. Note that the webpage is mainly in Chinese, though the second attachment of the webpage is a data description in English. Please contact the corresponding author if any assistance is needed.

The reviewer would also like to draw authors' attention to the following two recent papers, which are highly related to the focus of the current manuscript.
Zhang et al. [2019] reported double frequency modulation of electrons at keV and eV energy channels due to drift resonance and ExB force, respectively.
Shen et al. [2018] reported localized ULF waves in the noon to dusk sector of Earth's magnetosphere caused by foreshock transients

We would like to thank the reviewer for introducing recent papers on the relevant topic. In the revised manuscript, we include Zhang et al., 2019 in the discussion of "frequency doubling" in Section 4.4 and Shen et al., 2018 in the introduction section.

BD-IES Observation of Multi-Period Electron Flux Modulation Caused by Localized Ultra-Low Frequency Waves

Xingran Chen[1], Qiugang Zong[1], Hong Zou[1], Xuzhi Zhou[1], Li Li[1], Yixin Hao[1], and Yongfu Wang[1]

[1]Institute of Space Physics and Applied Technology, School of Earth and Space Sciences, Peking University, Beijing, China

Correspondence: Qiugang Zong (qgzong@pku.edu.cn) and Hong Zou (hongzou@pku.edu.cn)

Abstract. We present multi-period modulation of energetic electron flux observed by the BeiDa Imaging Electron Spectrometer (BD-IES) onboard a Chinese navigation satellite on October 13, 2015. Electron flux oscillations were observed at a dominant period of ∼190 s in consecutive energy channels from ∼50 keV to ∼200 keV. Interestingly, flux modulations at a secondary period of ∼400 s were also unambiguously observed. The oscillating signals at different energy channels were observed in sequence, with a time delay of up to ∼900 s. This time delay far exceeds the oscillating periods, by which we speculate that the modulations were caused by localized ultra-low frequency (ULF) waves. To verify the wave-particle interaction scenario, we revisit the classic drift-resonance theory. We adopt the calculation ~~scheme~~ **method** therein to derive the electron energy change in a multi-period ULF wave field. Then, based on the modeled energy change, we construct the flux variations to be observed by a virtual spacecraft. The predicted particle signatures well agree with the BD-IES observations. We demonstrate that the particle energy change might be underestimated in the conventional theories, as the Betatron acceleration induced by the curl of the wave ~~electron~~ **electric** field was often omitted. In addition, we show that azimuthally localized waves would notably extend the energy width of the resonance peak, whereas the drift-resonance interaction is only efficient for particles at the resonant energy in the original theory.

1 Introduction

Magnetospheric ultra-low frequency (ULF) waves, also known as geomagnetic pulsations, are plasma waves in the frequency range of ∼1 mHz to 1 Hz. Since the start of the space age, ULF waves have been extensively observed and widely regarded as hydromagnetic waves (e.g. Brown et al., 1961; Chen and Hasegawa, 1974; Kivelson and Southwood, 1985; Zong et al., 2017). These waves are found to play an important role in particle transport and acceleration in the solar terrestrial system (e.g. Hudson et al., 2001; Zong et al., 2009; Claudepierre et al., 2013; Foster et al., 2015). Particularly, ULF waves in the Pc 3-5 bands (Jacobs et al., 1964) can effectively interact with energetic particles via drift-resonance, as the period of the waves is comparable with the drift period of the particles (e.g. Elkington et al., 1999; Dai et al., 2013; Li et al., 2017a; Hao et al., 2019). As regards the drift-resonance wave-particle interaction, the energy transfer between the ULF waves and the energetic particles is most efficient for a specific energy, called the resonance energy, at which the particles would experience a ~~stable~~ **steady** electric field during their drift motion, thereby resulting in a cumulative net energy change.

Theoretical framework has been developed by Southwood and Kivelson (1981) to systematically understand the drift-resonance interaction between ULF waves and energetic particles. With the assumptions of an undisturbed particle trajectory and a monochromatic wave which has an infinitely small growth rate, they analytically derived the energy gain of the particle in the ULF wave field and the corresponding signature to be observed by a particle detector. According to their theory, particle flux observed at a fixed location would oscillate with large amplitude at the resonant energy and the resonant particle flux would be in anti-phase with respect to the azimuthal electric field of the wave. At lower or higher energies, the amplitude of the flux oscillation would rapidly decrease and the phase difference between the particle flux and the azimuthal electric field would be $\pm 90°$. In other words, the phase shift across the resonant energy would be $180°$. The amplitude profile and phase relationship of the flux modulation have been widely used as characteristic signatures to identify the drift-resonance interaction (e.g. Claudepierre et al., 2013; Hao et al., 2014; Chen et al., 2016). This conventional drift-resonance theory has been recently adapted by Zhou et al. (2015, 2016). They introduced a finite growth rate, as well as a finite damping rate, to describe the whole lifespan of the ULF wave in a more realistic way. In the case of their modified wave field, the phase shift of the particle fluxes across the resonant energy would be in the range from $90°$ to $180°$, depending on the evolution of the wave amplitude. This modified signature of drift-resonance has been verified by spacecraft observations (e.g. Zhou et al., 2015; Chen et al., 2016; Li et al., 2017a). In addition, ULF waves in the magnetosphere have been found to be ~~asymmetrically distributed~~ **azimuthally localized (e.g. Takahashi et al., 1985; Liu et al., 2009; Shen et al., 2018; Barani et al., 2019)**, whereas a ~~symmetric~~ **uniform** ULF wave field is assumed in the conventional drift-resonance theory. Li et al. (2017b) newly introduced a von Mises function into the drift-resonance theory to describe the ~~azimuthal asymmetry~~ **localized characteristics** of the ULF wave. They applied the revised theory to a previously reported event (Li et al., 2017a) and found that the observed particle signatures were better reproduced with the ~~asymmetric~~ **localized** ULF wave. The localized drift-resonance scenario is also addressed by Hao et al. (2017). They reported "boomerang stripes" observed by the Van Allen Probes (Blake et al., 2013; Mauk et al., 2013) and attributed the newly discovered features in the particle flux modulation to the interaction between relativistic electrons and localized poloidal ULF waves. The azimuthally localized nature of the ULF waves implies the possibility that energetic particles may interact with different waves along their drift trajectory, though it has rarely been reported.

In this paper, we present a case study of energetic electron flux modulated by ULF waves. Multi-period oscillations are unambiguously identified in the electron fluxes observed by BD-IES (Zong et al., 2018). We propose a natural and straightforward explanation that the flux variations were caused by multiple localized ULF waves at different periods. In the context of limited observations, we validate the localized wave-particle interaction scenario with a comparison between the observational signatures and the theoretical prediction of adiabatic energy change and particle flux. First, we revisit the ~~origin~~ **original** drift-resonance theory by Southwood and Kivelson (1981) and its recent extensions (Zhou et al., 2016; Li et al., 2017b) and fix a flaw in these prevailing drift-resonance theories. We show that the Betatron acceleration caused by the curl of the wave electric field, which is omitted in these theories, is comparable with the energy change caused by the poloidal electric field along the drift trajectory of the particle. The flawed theories, in general, can still give the correct characteristic phase relationship and amplitude profile of the particle flux modulation but overestimate the strength of the wave electric field. Then, with the corrected theory, we calculate the adiabatic energy change and the electron flux variation. It is found that the theoretically pre-

dicted signatures are in agreement with the BD-IES observations. Also, we present possible circumstantial evidence provided by ground-based magnetometers. Besides, we briefly discuss the width of the resonant amplitude peak and its relation to the azimuthal extent of the localized ULF waves.

2 Data

The electron flux data in this study are obtained by the BeiDa Imaging Electron Spectrometer (BD-IES) onboard a 55° inclined geosynchronous orbit (IGSO) spacecraft of China. This instrument, built by Peking University, employs a PIN-hole technique (Zou et al., 2013) and an anti-proton contamination design (Luo et al., 2015) to measure the differential electron flux from ∼50 keV to ∼600 keV in 8 energy channels (Zou et al., 2018a, b). The centroids of the channels are 59 keV, 80.5 keV, 111.5 keV, 150 keV, 205 keV, 280 keV, 380 keV, and 520 keV, respectively. The temporal resolution of the flux measurement is ∼10 s. The ground-based magnetometer data are provided by NASA's Space Physics Data Facility and INTERMAGNET at the cadence of 1 second.

3 Observation

Figure 1 presents an overview of the electron flux obtained by BD-IES on October 13, 2015. The IGSO spacecraft with BD-IES onboard passes through the radiation belt twice per orbit. Figures 1a and 1b show the electron flux in a full pass of the spacecraft through the radiation belt in the format of spectrogram and series **~~plot~~ plots** respectively. The multi-period modulation of the energetic electron fluxes was observed from ∼10:15 UT to ∼ 11:00 UT when the spacecraft traveled into the outer radiation belt. A zoomed-in view of the event is shown in Figure 1c. The colored solid lines represent the omni-directional differential electron fluxes while the black dotted lines refer to the 190 s running averaged fluxes. The flux modulations at the dominant period of ∼190 s, as well as the secondary oscillation at ∼400 s, are readily apparent. Figure 1d provides a zoomed-in view of Figure 1c to have a closer look at the multi-period oscillations in the 150 keV electron flux. Note that the secondary flux oscillation was barely significant at 150 keV, while the dominant ∼190 s modulation was observed in at least 4 consecutive energy channels from 59 keV to 150 keV. This difference is discussed in section 4.3 and attributed to the different azimuthal extent of the localized ULF waves.

Figure 2 shows the wavelet power spectrum (Grinsted et al., 2004) in order to quantitatively compare the amplitudes of the flux modulations at different periods and across the energy channels. The horizontal dashed lines in black and white mark the wave periods of 400 s and 190 s respectively. The comparison of the modulation amplitude across different energy channels is usually made by calculating the residuals of the particle fluxes (e.g. Claudepierre et al., 2013; Chen et al., 2016; Hao et al., 2017). The residual flux, defined as $\frac{J-J_0}{J_0}$, represents the flux variation normalized to the background flux so that the relative change of the particle flux caused by the waves can be quantitatively compared across different energy channels. Here J is the original differential flux obtained by the particle detector at a certain energy channel and J_0 is the corresponding **~~averaged flux~~ background flux which can be represented by the running averaged flux (e.g. Claudepierre et al., 2013; Hao et al., 2017)**.

Unfortunately, the residual flux is hard to derive in our event. For one thing, it is difficult to choose a proper width of the averaging window to calculate the averaged flux, since multi-period oscillations were observed. For another, a sharp increase of electron flux was observed at ∼10:05 UT when the spacecraft traveled across the outer boundary of the radiation belt. False signatures would be included if J_0 is obtained by any running averaging procedure. Therefore, the comparison of the modulation amplitude is alternatively achieved in our study by a careful selection of the colorbars to display the wavelet power spectrum. As the wavelet power is proportional to the square of the oscillation amplitude (Torrence and Compo, 1998), the upper limit of the colorbar for each energy channel is chosen to be the square of the mean value of the electron flux in the selected interval from 10:15 UT to 11:15 UT and the widths of the colorbars are consistently set to be 2. In this case, the same color in the wavelet power spectra refers to the same relative change of the electron flux. As shown in Figure 2, the flux modulation at the period of ∼190 s can be clearly identified in 4 consecutive energy channels from 59 keV to 150 keV. The oscillation at ∼400 s is evidently observed at 150 keV. This secondary oscillation can still be weakly recognized at 111.5 keV, but not at other energy channels. Besides, the electron flux modulation exhibits a **energy** dispersive characteristic. Oscillations were first observed in the 150 keV energy channel at ∼10:15 UT. For lower energies from 111.5 keV to 59 keV, the electron flux oscillations were observed afterwards, with increasing time delays of up to ∼15 minutes.

In the following section, we revisit the drift-resonance theory to seek a possible explanation for these observed particle signatures.

4 Discussion

4.1 Drift-Resonance Theory Revisited

In the original drift-resonance theory, Southwood and Kivelson (1981) proposed a path-integral approach to study the particle behavior in transverse ULF waves. The energy gain of a charged particle in the equatorial plane is calculated by integrating $q\boldsymbol{E}\cdot\boldsymbol{v}_d$ along the unperturbed particle drift orbit, where q and $\boldsymbol{v}_d$ denote the charge and drift velocity of the particle respectively. The wave electric field $\boldsymbol{E}$ is described by a monochromatic plane wave $E_\varphi \boldsymbol{e}_\varphi = E_0 \exp\left[\mathrm{i}\left(m\varphi - \omega t\right)\right]\boldsymbol{e}_\varphi$, where ω is the angular frequency, m is the azimuthal wave number, and E_0 is a constant that describes the amplitude of the wave. Here and throughout the paper, the equations are presented in cylindrical coordinates (r, φ, z). For a symmetric background magnetic field, the unperturbed drift orbit of an ~~**equatorial**~~ **equatorially** mirroring particle can be given by $r = r_0$, $\varphi = \varphi_0 + \omega_d t$, and $\omega_d = \frac{v_d}{r} = \frac{1}{r}\frac{\mu}{\gamma q}\frac{\nabla B}{B}$, where μ is the first adiabatic invariant, γ is the Lorentz factor, and (r_0, φ_0) is the initial position. Note that it is impractical to postulate a constant wave amplitude in which case any integration in time would strongly depend on the initial conditions. In practice, Southwood and Kivelson (1981) introduced a positive, infinitely small, and time-independent imaginary part of wave angular frequency by $\omega = \omega_r + \mathrm{i}\zeta$, where $\frac{\zeta}{\omega_r} \ll 1$. Then, the particle energy gain from the wave can be obtained by an integral along the unperturbed drift trajectory backwards till the time when the amplitude of the wave is negligible:

$$\delta W = \int_L q\boldsymbol{E}\cdot\boldsymbol{v}_d dt \propto -\frac{\mathrm{i}}{\omega - m\omega_d} E_\varphi. \tag{1}$$

For particles of a specific energy, called the resonant energy, that satisfies $m\omega_d = \omega_r$, the fraction $-\frac{\mathrm{i}}{\omega - m\omega_d}$ equals to $-\frac{1}{\zeta}$ which is a large negative real number. That is to say, the energy change of the particle would oscillate at large amplitude in anti-phase with the wave electric field. For lower or higher energies, the denominator is dominated by its real part, so that the energy change is $\mp 90^\circ$ out of phase with the wave electric field. With further assumption of constant energy and spatial gradients, the variation of particle flux is in proportion to the energy change. Therefore, particle flux modulation caused by drift-resonance would present a characteristic 180° phase shift across the resonant energy.

Recent adaption of the drift-resonance theory adopted the unperturbed path integral ~~scheme~~ **method** but introduced variations to E_0 and ζ to describe the spatial distribution and temporal evolution of the wave in a more realistic way. Zhou et al. (2015, 2016) considered a finite time-dependent ζ and showed that the phase shift of the electron flux oscillation across the resonant energy is time-dependent. The phase shift would grow from down to 90° at the beginning and become 180° when the wave amplitude reaches its maximum. Then, when the wave starts damping, the phase shift would keep growing as the drift velocities of the particles depend on their energies. This characteristic phase relationship is presented as "increasing tilted stripes" in the particle flux spectrogram. Li et al. (2017b) introduced an analog of Gaussian envelop to E_0 in the azimuthal dimension. Because it takes different times for particles of different energies to drift from the wave active region to the detector, a time delay between the particle fluxes observed at different channels would arise from this time-of-flight effect. In terms of phase, the time delay enlarges the initial phase shift across the resonant energy.

While the characteristic particle signatures of drift-resonance predicted by these prevailing theories have been proved by recent spacecraft observations, the particle energy change therein is derived in an incomplete way. In the guiding center approximation (Northrop, 1961), the rate of particle energy change averaged over a gyration is given by $\frac{dW}{dt} = q\boldsymbol{E}\cdot\boldsymbol{u} + \frac{\mu}{\gamma}\frac{\partial B}{\partial t}$, where $\boldsymbol{u}$ is the velocity of the guiding center (Northrop, 1963). For the unperturbed motion of an equatorially mirroring particle in a dipole-like magnetic field, $\boldsymbol{u}$ equals to the drift velocity $\boldsymbol{v}_d$. Hence, $q\boldsymbol{E}\cdot\boldsymbol{v}_d$ represents the rate of energy change caused by the wave electric field along the unperturbed guiding center trajectory. The Betatron acceleration caused by the curl of the wave electric field, denoted by $\frac{\mu}{\gamma}\frac{\partial B}{\partial t}$, is **wrongly** omitted in those drift-resonance theories (**e.g. Zhou et al., 2015, 2016; Li et al., 2017b**). ~~**One might neglect this energy change, because the magnetic field of fundamental mode waves has a node at the equator. Especially in the case of a purely poloidal wave, the perpendicular component of the wave magnetic field B_r can be identically zero in the equatorial plane. However, even then, there would still be a non-negligible change of magnetic field magnitude, because there should be a parallel wave magnetic field B_z according to the Faraday's law. Therefore, this $\nabla\times\boldsymbol{E}$ induced energy change should be included in the integral to obtain the total kinetic energy change of the particle.**~~ Note that, for poloidal waves, $\nabla\times\boldsymbol{E}$ is controlled by $\frac{\partial E}{\partial r}$, since $\boldsymbol{E}$ is in the azimuthal direction. Consequently, the particle energy change would be greatly influenced by the radial gradient of wave electric field amplitude, although the particle drifts at a constant L shell in the unperturbed orbit approximation. Observational and modeling studies showed that the power of ULF wave electric field generally increases with radial distance within the outer radiation belt region (e.g. Perry et al., 2005; Ozeke et al., 2012, 2014) and is structured by plasma density inhomogeneities (e.g. Degeling et al., 2018). In the following discussions, we amend the omissions in the previous drift-resonance theories, while retaining the unperturbed orbit approximation for the simplicity of calculation.

We confine our discussion in the equatorial plane. The background field is given by $\boldsymbol{B}_0 = B_0\boldsymbol{e}_z = \frac{B_E}{L^3}\boldsymbol{e}_z$ where B_E is magnitude of the equatorial magnetic field at the Earth's surface. In this case, the particle drift velocity $\boldsymbol{v}_d$ equals to $-\frac{\mu}{\gamma q}\frac{3}{r}\boldsymbol{e}_\varphi$. The poloidal ULF wave fields can be given ~~in a general form~~ by $\boldsymbol{E}_1 = -\frac{\partial A}{\partial t}\boldsymbol{e}_\varphi \triangleq E_\varphi \boldsymbol{e}_\varphi$ and $\boldsymbol{B}_1 = \nabla \times (A\boldsymbol{e}_\varphi) = -\frac{\partial A}{\partial z}\boldsymbol{e}_r + \frac{1}{r}\frac{\partial (rA)}{\partial r}\boldsymbol{e}_z$, where $\boldsymbol{A} = A\boldsymbol{e}_\varphi$ is the magnetic vector potential. Then, the rate of particle energy change caused by the electric field along the unperturbed path of its guiding center is denoted by:

$$q\boldsymbol{E}\cdot\boldsymbol{v}_d = \frac{\mu}{\gamma}\frac{3}{r}\frac{\partial A}{\partial t} = -\frac{\mu}{\gamma}\frac{3}{r}E_\varphi. \tag{2}$$

For fundamental mode waves, it is reasonable to further assume that the amplitude of the wave does not vary in the vicinity of equator (i.e. $\frac{\partial A}{\partial z} = 0$). Then, the wave magnetic field would only have a parallel component, in which case the Betatron acceleration term can be calculated by:

$$\frac{\mu}{\gamma}\frac{\partial B}{\partial t} = \frac{\mu}{\gamma}\frac{\partial}{\partial t}\frac{\partial (rA)}{\partial r} = -\frac{\mu}{\gamma}\left(\frac{1}{r} + \frac{1}{E_\varphi}\frac{\partial E_\varphi}{\partial r}\right)E_\varphi. \tag{3}$$

One may easily find that the total rate of particle energy change is in proportion to $q\boldsymbol{E}\cdot\boldsymbol{v}_d$:

$$\frac{dW}{dt} = q\boldsymbol{E}\cdot\boldsymbol{v}_d + \frac{\mu}{\gamma}\frac{\partial B}{\partial t} = -\frac{\mu}{\gamma}\left(\frac{4}{r} + \frac{1}{E_\varphi}\frac{\partial E_\varphi}{\partial r}\right)E_\varphi = \frac{4 + \frac{r}{E_\varphi}\frac{\partial E_\varphi}{\partial r}}{3}q\boldsymbol{E}\cdot\boldsymbol{v}_d. \tag{4}$$

In other words, the amendments do no change the characteristic phase relationship in the particle signatures, but alter the ratio between the strength of ULF wave field and particle energy modulation. Particularly, for the zeroth order approximation that the amplitude of the wave electric field does not change with radial distance (e.g. in the vicinity of the radial amplitude peak), the ~~the~~ fraction $\frac{4+\frac{r}{E_\varphi}\frac{\partial E_\varphi}{\partial r}}{3}$ equals to $\frac{4}{3}$. For the empirical electric field model denoted by $E_\varphi \propto \exp[\sigma r]$ (e.g. Perry et al., 2005; Ozeke et al., 2014), the fraction $\frac{4+\frac{r}{E_\varphi}\frac{\partial E_\varphi}{\partial r}}{3}$ equals to $\frac{4+\sigma r}{3}$, where σ is a constant factor in the order of 0.3 R_E^{-1} . In the outer radiation belt (e.g. $r = 6\ R_E$), $\frac{4+\sigma r}{3}$ is around 2, which means the negligence of $\frac{\mu}{\gamma}\frac{\partial B}{\partial t}$ can result in a $\sim 50\%$ underestimate of the particle energy change.

4.2 The Localized Drift-Resonance Scenario

As described in section 3, the electron flux modulations were first observed in the 150 keV energy channel at ~10:15 UT. The flux oscillations were observed sequentially afterwards in lower energy channels. According to Li et al. (2017b), this dispersive characteristic implies that the ULF waves were azimuthally confined and the particle detector was located outside the region of strong wave activity. Thus, it is natural to attribute the observed multi-period modulation to multiple localized ULF waves. In consideration of the limited observations, we reproduce the particle signatures observed by BD-IES to substantiate this localized wave-particle scenario. First, we assume a modeled ULF wave field and employ the integral ~~scheme~~ **method** described in section 4.1 to calculate the changes of electron energy. Then, the energy changes are transformed into flux variations to compare with the observations. More specifically, the magnetic vector potential of the modeled ULF wave is given by:

$$\boldsymbol{A} = A\boldsymbol{e}_\varphi = \sum_{n=1,2} A_i(r,\varphi,t)\,\boldsymbol{e}_\varphi = \sum_{n=1,2} A_{0,n}G_n(r)\,H_n(\varphi)\,F_n(\varphi,t)\,\boldsymbol{e}_\varphi, \tag{5}$$

where the subscripts 1 and 2 refer to the two modeled monochromatic ULF waves. **For each of the monochromatic wave,** the constant factor $A_{0,n}$ denotes **its amplitude ~~the amplitude of the wave~~**. The second term $G_n(r)$ **~~describe~~ describes the distribution** of wave amplitude in the radial direction. The third term $H_n(\varphi) = \frac{\exp[\xi_n \cos(\varphi - \varphi_{0,n})]}{2\pi I_0(\xi_n)}$ is a von Mises function, describing the azimuthal distribution of the ULF wave (Li et al., 2017b). Here $\varphi_{0,n}$ is the central azimuth of the wave active region, ξ_n is the concentration parameter, and $I_0(\xi_n)$ is the zeroth-order modified Bessel function **of the first kind**. The von Mises distribution is an analogue of the normal distribution for a periodic variable. For a large positive ξ, the distribution is highly concentrated, whereas when ξ approaches zero, it reduces to a uniform distribution. The growth, damping, and propagation of the wave is described in the last term $F_n(\varphi, t)$ by:

$$F_n(\varphi,t) = \frac{\sqrt{\pi}}{2}\tau_{\pm,n}\exp\left[-\frac{\omega_n^2\tau_{\pm,n}^2}{4}\right]\mathrm{erf}\left[\frac{t-t_{0,n}}{\tau_{\pm,n}} + \frac{\omega_n\tau_{\pm,n}}{2}\mathrm{i}\right]\exp\left[\mathrm{i}\left(m_n\varphi - \omega_n t_{0,n} + \theta_{0,n}\right)\right] + C_n(\varphi), \tag{6}$$

where $\mathrm{erf}[\mathrm{z}] = \frac{2}{\sqrt{\pi}}\int_0^z \exp\left[-t^2\right]dt$ is the error function. ω_n, m_n, and $\theta_{0,n}$ are the frequency, azimuthal wave number, and initial phase, respectively. $t_{0,n}$ denotes the time when the wave amplitude reaches its maximum value. The wave grows/damps at the time-scale of $\tau_{+,n}/\tau_{-,n}$, synthesized as $\tau_{\pm,n}$ in Equation (6), before/after $t_{0,n}$. $C_n(\varphi)$ is a function independent of time given by:

$$\begin{aligned} C_n(\varphi) = {} & \frac{\sqrt{\pi}}{2}\tau_{+,n}\exp\left[-\frac{\omega_n^2\tau_{+,n}^2}{4}\right]\left(\mathrm{erf}\left[\frac{\omega_n\tau_{+,n}}{2}\mathrm{i}\right]+1\right)\exp\left[\mathrm{i}\left(m_n\varphi - \omega_n t_{0,n} + \theta_{0,n}\right)\right] \\ & - \frac{\sqrt{\pi}}{2}\tau_{\pm,n}\exp\left[-\frac{\omega_n^2\tau_{\pm,n}^2}{4}\right]\mathrm{erf}\left[\frac{\omega_n\tau_{\pm,n}}{2}\mathrm{i}\right]\exp\left[\mathrm{i}\left(m_n\varphi - \omega_n t_{0,n} + \theta_{0,n}\right)\right]. \end{aligned} \tag{7}$$

Since $\lim_{t\to-\infty}\mathrm{erf}\left[\frac{t-t_{0,n}}{\tau_{\pm,n}} + \frac{\omega_n\tau_{\pm,n}}{2}\mathrm{i}\right] = -1$, the choice of $C_n(\varphi)$ ensures an infinitely small wave amplitude at $t = -\infty$ for all azimuths ($\lim_{t\to-\infty} F(\varphi,t) = 0$). The wave electromagnetic fields are given by:

$$\begin{aligned} \boldsymbol{E} &= -\frac{\partial \boldsymbol{A}}{\partial t} = \sum_{n=1,2} A_{0,n}G_n(r)H_n(\varphi)\frac{\partial F_n(\varphi,t)}{\partial t}\boldsymbol{e}_\varphi \\ &= \sum_{n=1,2} A_{0,n}G_n(r)H_n(\varphi)\exp\left[-\frac{(t-t_{0,n})^2}{\tau_{\pm,n}^2}\right]\exp\left[\mathrm{i}\left(m_n\varphi - \omega_n t + \theta_{0,n}\right)\right]\boldsymbol{e}_\varphi \end{aligned} \tag{8}$$

and

$$\begin{aligned} \boldsymbol{B} &= \nabla\times\boldsymbol{A} = \frac{1}{r}\frac{\partial(rA)}{\partial r}\boldsymbol{e}_z = \left(\frac{1}{r} + \frac{1}{A}\frac{\partial A}{\partial r}\right)A\boldsymbol{e}_z \\ &= \sum_{n=1,2} A_{0,n}\left(\frac{1}{r} + \frac{1}{G_n}\frac{\partial G_n}{\partial r}\right)G_n(r)H_n(\varphi)F_n(\varphi,t)\,\boldsymbol{e}_z. \end{aligned} \tag{9}$$

We adopt a set of parameters (somewhat arbitrarily to fit the particle signatures observed by BD-IES) as follows: $A_{0,1} =$ 1.1 mV/m, $m_1 = 20$, $\omega_1 = \frac{2\pi}{190}$, $\xi_1 = 16$, $\varphi_{0,1} = -\frac{5\pi}{12}$, $t_{0,1} = 600$ s, $\theta_{0,1} = -\frac{3\pi}{5}$, $\tau_{+,1} = 200$ s and $\tau_{-,1} = 800$ s; $A_{0,2} = 0.2$ mV/m, $m_2 = 7$, $\omega_2 = \frac{2\pi}{400}$, $\xi_2 = 1$, $\varphi_{0,2} = -\frac{\pi}{3}$, $t_{0,2} = 1100$ s, $\theta_{0,2} = 0$, $\tau_{+,2} = 400$ s and $\tau_{-,2} = 600$ s. Here $t = 0$ and $\varphi = 0$ correspond to 10:00 UT and 15:00 MLT, respectively. Since our calculation would be confined to the unperturbed particle

orbit at $r_0 = 7\ R_E$ (consistent with the spacecraft position), we parameters describing the radial distribution of the wave amplitude are simply set as $G_{1,2}(r_0) = 1$. The modeled electromagnetic fields, which consists of two localized ULF waves, are shown in Figures 3a and 3b. In view of the striking difference of the amplitude, we also show the normalized characteristics of the two monochromatic waves separately. We present the electromagnetic fields in the form of separation of variables by $E_n = E_n^*(t) H_n(\varphi) \exp[\mathrm{i}m_n\varphi]$ and $B_n = B_n^*(t) H_n(\varphi) \exp[\mathrm{i}m_n\varphi]$. The temporal evolution of the waves $E_n^*(t)$ are shown in Figures 3c, 3d, 3g, 3h. The azimuthal distribution of wave magnitude $H_n(\varphi)$ are shown in Figures 3e and 3i. The different azimuthal concentration of the two monochromatic waves ($\xi_1 = 16$ and $\xi_2 = 1$) would cause a difference in the energy width of the modulated particles. The wider azimuthal extent of the 400 s wave may explain the narrower energy range of the electron flux modulation in the particle spectrum observed by BD-IES, which will be discussed in detail in section 4.3.

To verify the localized drift-resonance scenario, we numerically calculate the energy change of the electrons caused by the modeled ULF wave and predict the particle signatures to be observed by a virtual spacecraft. The orange dashed lines in Figure 3 mark the position of the virtual spacecraft which is away from the regions of strong wave activities. Specifically, the virtual spacecraft is placed at $\varphi = \frac{\pi}{4}$, while the central positions of the wave active regions are $\varphi_{0,1} = -\frac{5\pi}{12}$ and $\varphi_{0,2} = -\frac{\pi}{3}$. The azimuthal of the virtual spacecraft corresponds to $MLT = 18$, in consistence with the position of BD-IES in our event. Figure 4a shows the relative energy change of the electrons. Multi-period patterns are readily apparent at ~150 keV. The final step to achieve comparison between theory and observation is transforming the calculated energy changes into particle flux variations. According to Zhou et al. (2016) and Li et al. (2017b), the transformation can be performed in two steps. First, the variation of phase space density is derived from the energy change, provided a power law spectrum of the electrons ($f \propto W^{-n}$). Then, the change of phase space density can be further transformed into the flux variation following the standard relationship $f = \frac{j}{p^2}$, where j is the flux and p is the particle momentum (e.g. Hilmer et al., 2000; Chen et al., 2005; Roederer and Zhang, 2014). Note that the relative changes of the phase space density $\left(\frac{df}{f}\right)$ and the particle flux $\left(\frac{dj}{j}\right)$ are essentially equivalent (e.g. Zhou et al., 2016; Chen et al., 2016; Li et al., 2017b). The calculated phase space density change under the localized drift-resonance scenario is shown in Figure 4b. Here the power law exponent n equals to 2.5 in our calculation, and the widths of the energy channels of the virtual spacecraft are identical to those of BD-IES. A comparison between the results of our numerical calculation and the BD-IES observations is presented in Figures 4c and 4d. The triangles mark the modulation peaks. It is shown that the multi-period particle signatures are well reproduced by our numerical calculation.

Besides the particle signatures, ground-based magnetic field observations can provide circumstantial evidences to the localized drift-resonance scenario, although we lack the accompanied in-situ electromagnetic field observations. The spacecraft with BD-IES onboard was located in the southern hemisphere with its footpoint mapped at $\sim 66^\circ S$ geographic latitude during the event. In the vicinity of the $\sim 66^\circ$ isopleth, we find three geomagnetic stations, tagged PG4, CSY, and DRV, that provided 3-dimensional magnetic field measurements. The stations were located on Antarctica, southern to the spacecraft footpoint, which means that they ~~corresponds~~ **correspond** to a slightly higher L shell than BD-IES. For the two stations in the dusk sector, CSY and DRV, closer to the footpoint of BD-IES in the longitudinal direction, no ULF perturbation in the Pc 3-5 band were observed. Meanwhile, the PG4 station located in the noon sector observed large amplitude ULF waves. The observation of ULF waves away from the footpoint of BD-IES and the absence of wave activities in the vicinity of the footpoint support

the idea that the ULF waves in our event were restricted to azimuthally limited regions. (See Figures S1 and S2 in supporting information for more details.)

4.3 The Resonance Width

In the drift-resonance scenario, the amplitude of the flux oscillate peaks at the resonance energy and rapidly decreases at lower or higher energies. The resonance width describes the energy extent of this amplitude peak. For a global monochromatic wave with an infinitely small growth rate, the energy change oscillation is theoretically restricted to the resonant energy with an infinitely narrow width. However, flux oscillations observed by actual particle detectors usually show finite resonance widths. As pointed out by previous studies, the resonance width depends on the widths of the energy channels (e.g. Southwood and Kivelson, 1981), particle phase space density gradient (e.g. Zhou et al., 2016; Chen et al., 2016), and growth rate of the wave (e.g. Zhou et al., 2015). We propose that the azimuthal extent of the localized ULF waves also plays an important role in the resonance width under the localized drift-resonance scenario. Figure 5 shows an example of the particle signatures in response to the localized ULF waves of different azimuthal distributions. The only difference among the wave fields shown in Figures 5a-5c is the concentration parameter ξ, whereas all other parameters are set the same. The corresponding particle signatures observed by the virtual spacecraft are shown in Figures 5d-5f. For an increasingly concentrated wave field (demonstrated by an increasing value of ξ), the width of the resonant amplitude peak extends. In other words, particles of a wider energy range can gain non-zero net energy changes from the highly localized waves. This broadened resonance width can be explained by the incomplete cancellation of the positive and negative energy changes. For a monochromatic ULF wave of azimuthally uniform distribution, a non-resonant particle experiences alternating electric fields during its drift motion. The gain and loss of the energy cancel each other out. However, for a localized ULF wave, a non-resonant particle may leave the region of strong wave activity with uncanceled energy change as it proceeds its azimuthal drift motion, which in turn results in a variation of the non-resonant particle flux.

4.4 Other Possible Scenarios and Future Work

Although the localized drift-resonance scenario applies well in our event, we do not rule out other possible explanations, considering the limited observations and the simplistic numerical calculation. The particle trajectory is assumed to be unperturbed while the electron gains and loses energy in the ULF wave field. This assumption would ~~not~~ be ~~valid~~ **invalid** for large amplitude waves which could alter the particle motion significantly. **Li et al. (2018) conducted a more more self-consistent analysis with the perturbed particle trajectory taken into account. They employed the pendulum equation to describe the particle motion and derived the corresponding energy change. According to their theory, multi-period oscillations of particle fluxes are expected to be observed near the resonant energy, as a large amplitude poloidal mode ULF wave would typically produce "rolled-up" structures in the particle energy spectrum.** ~~**A more self-consistent analysis with the perturbed particle trajectory taken into account is conducted in a separate study.**~~ Besides, the bounce motion of the particles is neglected in our simple calculation though the spacecraft with BD-IES onboard was located off the equatorial plane in our event. For bouncing particles, the interaction with ULF waves is more complicated even if we only consider the

drift-resonance process. In this case, not only the azimuthal distribution of the ULF electric field but also its morphology along the field line plays an important role in the wave-particle interaction. In addition, the ULF magnetic field can modify the pitch angle of the particle (e.g. Chaston et al., 2017, 2018), although the Lorentz force is perpendicular to the particle velocity and causes no energy change. Unfortunately, the pitch angle distribution of the energetic electrons observed by the BD-IES instrument has not yet been resolved. Hence, we focus on equatorial mirroring electrons since there has already been a bunch of parameters in our numerical calculation.

Additionally, multi-period signatures, especially the "frequency doubling" feature, have been investigated and attributed to several independent mechanisms. Higuchi et al. (1986) first reported this harmonic structure in the magnetic field observed by geostationary satellites. They proposed that the multi-period structure in the compressional component of the magnetic field was formed by requiring the balance of overall pressure as there existed a modulation of the plasmas by the magnetic field. Other possible causes of the "frequency doubling" signatures include the periodic motion of the field line nodes (Takahashi et al., 1987), nonlinear drift-bounce resonance (Southwood and Kivelson, 1997), ballooning-mirror mode instability (Sibeck et al., 2012), **and** $E \times B$ **effect (Zhang et al., 2019)**. As the secondary period of the flux modulation **observed by BD-IES in the present event** happened to be nearly twice the dominant period, it could be possible that the multi-period modulations of the electron fluxes were caused by ~~**nonlinear wave-particle interactions**~~ **either mechanism(s) mentioned above**.

5 Summary

We present BD-IES observations of multi-period electron flux modulations. Oscillations at the dominant period of $\sim$190 s were observed in 4 consecutive energy channels. Meanwhile, a $\sim$400 s secondary modulation was also unambiguously observed at 150 keV, as well as weakly identified at 111.5 keV. The observed particle signatures are attributed to the drift-resonance interaction between the energetic electrons and two localized ULF waves of different azimuthal distributions and different periods.

We revisit the theoretical scheme of drift-resonance developed by Southwood and Kivelson (1981) and its recent adaptations, and fix a flaw in the prevailing theories. We show that the Betatron acceleration caused by the curl of the wave electric field, often omitted in these theories, plays an non-negligible role in the modulation of particle fluxes. The amplitude of this induced modulation is comparable with the energy change caused by the electric field along the drift path of the particle. Fortunately, the flawed theories still give the correct characteristic phase relationship in the particle signatures, because the two terms of energy changes, $q\boldsymbol{E} \cdot \boldsymbol{v}_d$ and $\frac{\mu}{\gamma}\frac{\partial B}{\partial t}$ are in-phase. But the flawed theories might overestimate the strength of the wave electromagnetic fields, in the usual case that the wave amplitude increases with radial distance within the outer radiation belt.

Based on the modified drift-resonance theory, we reproduce the particle signatures observed by BD-IES with ~~**a**~~ **an** azimuthally confined modeled ULF wave of multi-periods. The well agreement between ~~**the**~~ our numerical calculation and the BD-IES observation demonstrates that multiple localized ULF waves can apply combined effects on the energetic particles, which is foreseeable by the localized drift-resonance theory but rarely reported in observations. In addition, the relationship

between the width of the resonant amplitude peak and the azimuthal extent of the wave active region is studied. We illustrate that highly localized ULF waves can cause net energy changes of the non-resonant particles due to the incomplete cancellation of the energy gains and losses in the alternating wave fields. Hence, the azimuthal concentration of the waves **~~extend~~ extends** the energy width of the resonance peak.

Author contributions. XC analyzes the observational data, conducts the numerical calculation, and prepares the manuscript. HZ is in charge of the BD-IES instrument. LL takes part in the theoretical derivation and numerical caluclation. QZ, XZ, YH, and YW discuss and revise the manuscript.

Competing interests. The authors declare that no competing interests are present.

Acknowledgements. This work was supported by the National Natural Science Foundation of China (41421003 and 41774168). Thanks Linlin Chen for revising the English syntax. The electron flux data of BD-IES are available at http://www.space.pku.edu.cn/bd-ies/BD_IES_OVERVIEW.html. The ground-based magnetometer data used in this paper is downloaded from NASA's Space Physics Data Facility (http://spdf.gsfc.nasa.gov/) and INTERMAGNET (http://www.intermagnet.org).

References

Barani, M., Tu, W., Sarris, T., Pham, K., and Redmon, R. J.: Estimating the azimuthal mode structure of ULF waves based on multiple GOES satellite observations, J. Geophys. Res., 124, 5009-5026. doi:10.1029/2019JA026927, 2019

Blake J. B., et al.: The magnetic electron ion spectrometer (MagEIS) instruments aboard the radiation belt storm probes (RBSP) spacecraft, Space Sci. Rev., 179, 383-421, 2013.

Brown, R. R., et al.: Large-scale electron bombardment of the atmosphere at the sudden commencement of a geomagnetic storm, J. Geophys. Res., 66(4), 1035-1041, doi:10.1029/JZ066i004p01035, 1961.

Chaston, C. C., Bonnell, J. W., Wygant, J. R., Reeves, G. D., Baker, D. N., Melrose, D. B., and Cairns, I. H.: Radial transport of radiation belt electrons in kinetic field-line resonances, Geophys. Res. Lett., 44, 8140-8148, doi:10.1002/2017GL074587, 2017.

Chaston, C. C., Bonnell, J. W., Wygant, J. R., Reeves, G. D., Baker, D. N., Melrose, D. B.: Radiation belt "dropout" and drift-bounce resonances in broadband electromagnetic waves, Geophys. Res. Lett., 45, 2128-2137, doi:10.1002/2017GL076362, 2018.

Chen, L. and Hasegawa, A.: A theory of long-period magnetic pulsations: 1. Steady state excitation of field line resonance, J. Geophys. Res., 79, 1024-1032, doi:10.1029/JA079i007p01024, 1974.

Chen, X.-R., Zong, Q.-G., Zhou, X.-Z., Blake, J. B., Wygant, J. R., and Kletzing, C. A.: Van Allen Probes observation of a 360° phase shift in the flux modulation of injected electrons by ULF waves, Geophys. Res. Lett., 43, 1614-1624, doi:10.1002/2016GL071252, 2016.

Chen, Y., et al.: Multisatellite determination of the relativistic electron phase space density at geosynchronous orbit: Methodology and results during geomagnetically quiet times, J. Geophys. Res., 110, A10210, doi:10.1029/2004JA010895, 2005.

Claudepierre, S. G., et al.: Van Allen Probes observation of localized drift resonance between poloidal mode ultra-low frequency waves and 60 keV electrons, Geophys. Res. Lett., 40, 4491-4497, 2013.

Dai, L., et al.: Excitation of poloidal standing Alfven waves through drift resonance wave-particle interaction, Geophys. Res. Lett., 40, 4127-4132, 2013.

Degeling, A. W., et al.: Control of ULF wave accessibility to the inner magnetosphere by the convection of plasma density, J. Geophys. Res., 123, 1086-1099, doi:10.1002/2017JA024874, 2018.

Elkington, S. R., Hudson, M. K., and Chan, A. A.: Acceleration of relativistic electrons via drift-resonant interaction with toroidal-mode Pc-5 ULF oscillations, Geophys. Res. Lett., 26, 3273-3276, doi:10.1029/1999GL003659, 1999.

Foster, J. C., Wygant, J. R., Hudson, M. K., Boyd, A. J., Baker, D. N., Erickson, P. J., and Spence, H. E.: Shock-induced prompt relativistic electron acceleration in the inner magnetosphere, J. Geophys. Res., 120, 1661-1674, doi:10.1002/2014JA020642, 2015.

Grinsted, A., Moore, J. C., and Jevrejeva, S.: Application of the cross wavelet transform and wavelet coherence to geophysical time series, Nonlin. Processes Geophys., 11, 561-566, 2004.

Hao, Y.-X., et al.: Interactions of energetic electrons with ULF waves triggered by interplanetary shock: Van Allen Probes observations in the magnetotail, J. Geophys. Res., 119, 8262-8273, doi:10.1002/2014JA020023, 2014.

Hao, Y.-X., Zong, Q.-g., Zhou, X.-Z., Rankin, R., Chen, X.-R., Liu, Y., Fu, S.-Y., Spence, H. E., Blake, J. B., and Reeves, G. D.: Relativistic electron dynamics produced by azimuthally localized poloidal mode ULF waves: Boomerang-shaped pitch angle evolutions, Geophys. Res. Lett., 44, 7618-7627, doi:10.1002/2017GL074006, 2017.

Hao, Y.-X., Zong, Q.-G., Zhou, X.-Z., Rankin, R., Chen, X.-R., Liu, Y. et al.: Global-scale ULF waves associated with SSC accelerate magnetospheric ultrarelativistic electrons, J. Geophys. Res., 124, doi:10.1029/2018JA026134, 2019.

Higuchi, T., Kokubun, S., and Ohtani, S.: Harmonic structure of compressional Pc5 pulsations at synchronous orbit, Geophys. Res. Lett., 13, 1101-1104, doi:10.1029/GL013i011p01101, 1986.

Hilmer, R. V., Ginet, G. P., and Cayton, T. E.: Enhancement of equatorial energetic electron fluxes near L = 4.2 as a result of high speed solar wind streams, J. Geophys. Res., 105(A10), 23311-23322, doi:10.1029/1999JA000380, 2000.

Hudson, M. K., et al.: Radiation belt electron acceleration by ULF wave drift resonance: Simulation of 1997 and 1998 storms, in Space Weather, edited by Song, P., Singer, H. J., and Siscoe, G. L., vol. 125, p. 289, AGU, Washington, D. C., 2001.

Jacobs, J. A., Kato, Y., Matsushita, S., and Troitskaya, V. A.: Classification of geomagnetic micropulsations, J. Geophys. Res., 69(1), 180-181, doi:10.1029/JZ069i001p00180, 1964.

Kivelson, M. G. and Southwood, D. J.: Resonant ULF waves: A new interpretation, Geophys. Res. Lett., 12, 49-52, doi:10.1029/GL012i001p00049, 1985.

Li L., et al.: Ultralow frequency wave characteristics extracted from particle data: Application of IGSO observations, Sci. China Tech. Sci., 60, 419-424, doi:10.1007/s11431-016-0702-4, 2017a.

Li, L., Zhou, X.-Z., Zong, Q.-G., Rankin, R., Zou, H., Liu, Y., Chen, X.-R., and Hao, Y.-X.:, Charged particle behavior in localized ultralow frequency waves: Theory and observations, Geophys. Res. Lett., 44, 5900-5908, doi:10.1002/2017GL073392, 2017b.

Li, L., Zhou, X.-Z., Omura, Y., Wang, Z.-H., Zong, Q.-G., Liu, Y., et al.: Nonlinear drift resonance between charged particles and ultralow frequency waves: Theory and observations. Geophys. Res. Lett., 45, 8773-8782, doi:10.1029/2018GL079038, 2018.

Liu, W., Sarris, T. E., Li, X., Elkington, S. R., Ergun, R., Angelopoulos, V., Bonnell, J., and Glassmeier, K. H.: Electric and magnetic field observations of Pc4 and Pc5 pulsations in the inner magnetosphere: A statistical study, J. Geophys. Res., 114, A12206, doi:10.1029/2009JA014243, 2009.

Luo, L., Zou, H., and Zong, Q.-G., et al.: Anti-proton contamination design of the imaging energetic electron spectrometer based on Geant4 simulation, Sci. China Tech. Sci., 58, 1385-1391, 2015.

Mauk, B. H., et al.: Science objectives and rationale for the Radiation Belt Storm Probes mission, Space Sci. Rev., 179, 3-27, doi:10.1007/s11214-012-9908-y, 2013.

Northrop, T. G.: The guiding center approximation of charged particle motion, Annals of Physics, 15(1), 79-101, doi:10.1016/0003-4916(61)90167-1, 1963.

Northrop, T. G.: Adiabatic charged-particle motion, Reviews of Geophysics, 1, 283-304, doi:10.1029/RG001i003p00283, 1963.

Ozeke, L. G., et al.: ULF wave derived radiation belt radial diffusion coefficients, J. Geophys. Res., 117, A04222, doi:10.1029/2011JA017463, 2012.

Ozeke, L. G., et al.: Analytic expressions for ULF wave radiation belt radial diffusion coefficients, J. Geophys. Res., 119, 1587-1605, doi:10.1002/2013JA019204, 2014.

Perry, K. L., Hudson, M. K., and Elkington, S. R.: Incorporating spectral characteristics of Pc5 waves into three-dimensional radiation belt modeling and the diffusion of relativistic electrons, J. Geophys. Res., 110, A03215, doi:10.1029/2004JA010760, 2005.

Roederer, J. G. and Zhang, H.: Dynamics of Magnetically Trapped Particles (Second Edition), Springer-Verlag, Berlin Heidelberg, 2014.

Shen, X.-C., Shi, Q., Wang, B., Zhang, H., Hudson, M. K., Nishimura, Y., et al.: Dayside magnetospheric and ionospheric responses to a foreshock transient on 25 June 2008: 1. FLR observed by satellite and ground-based magnetometers, J. Geophys. Res., 123, 6335-6346, doi:10.1029/2018JA025349, 2018.

Sibeck, D. G., Korotova, G., Turner, D. L., Angelopoulos, V., Glassmeier, K. H., and McFadden, J. P.: Frequency doubling and field-aligned ion streaming in a long-period poloidal pulsation, J. Geophys. Res., 117, A11215, doi:10.1029/2011JA017473, 2012.

Southwood, D. J. and Kivelson, M. G.: Charged particle behavior in low-frequency geomagnetic pulsations 1. Transverse waves, J. Geophys. Res., 86(A7), 5643-5655, 1981.

Southwood, D. J. and Kivelson, M. G.:, Frequency doubling in ultralow frequency wave signals, J. Geophys. Res., 102, 27151-27158, 1997.

Takahashi, K., Higbie, P. R., and Baker, D. N.: Azimuthal propagation and frequency characteristic of compressional Pc 5 waves observed at geostationary orbit, J. Geophys. Res., 90(A2), 1473-1485, doi:10.1029/JA090iA02p01473, 1985.

Takahashi, K., Zanetti, L. J., Potemra, T. A., and Acuna, M. H.: A model for the harmonic of compressional Pc 5 waves, Geophys. Res. Lett., 14, 363-366, doi:10.1029/GL014i004p00363, 1987.

Torrence, C. and Compo, G. P.: A Practical Guide to Wavelet Analysis, Bull. Amer. Meteor. Soc., 79, 61-78, 1998.

Zhang, S., Tian, A., Degeling, A. W., Shi, Q., Wang, M., Hao, Y., et al.: Pc4-5 Poloidal ULF Wave Observed in the Dawnside Plasmaspheric Plume. J. Geophys. Res., 124, 9986-9998, doi:10.1029/2019JA027319, 2019.

Zhou, X.-Z., et al.: Imprints of impulse-excited hydromagnetic waves on electrons in the Van Allen radiation belts, Geophys. Res. Lett., 42(15), 6199-6204, 2015.

Zhou, X.-Z., et al.: Charged particle behavior in the growth and damping stages of ultralow frequency waves: Theory and Van Allen Probes observations, J. Geophys. Res., 121, 3254-3263, doi:10.1002/2016JA022447, 2016.

Zong, Q.-G., et al.: Ultralow frequency modulation of energetic particles in the dayside magnetosphere, Geophys. Res. Lett., 34, L12105, doi:10.1029/2007GL029915, 2007.

Zong, Q.-G., et al.: Energetic electron response to ULF waves induced by interplanetary shocks in the outer radiation belt, J. Geophys. Res., 114, A10204, doi:10.1029/2009JA014393, 2009.

Zong, Q.-G., Rankin, R., and Zhou, X.-Z.: The interaction of ultra-low-frequency pc3-5 waves with charged particles in Earth's magnetosphere, Rev. Mod. Plasma Phys., 1, doi:10.1007/s41614-017-0011-4, 2017.

Zong, Q., Wang, Y., Zou, H., Wang, L., Rankin, R., and Zhang, X.: New magnetospheric substorm injection monitor: Image electron spectrometer on board a Chinese navigation IGSO satellite, Space Weather, 16, 121-125, doi:10.1002/2017SW001708, 2018.

Zou, H., Luo, L., and Li, C.-F., et al.: Angular response of 'pin-hole' imaging structure measured by collimated β source, Sci. China Tech. Sci., 56, 2675-2680, 2013.

Zou, H., et al.: Monte Carlo simulations of the sensor head of Imaging energetic Electron Spectrometer onboard a Chinese IGSO navigation satellite, Sci. China Tech. Sci., 62, 1169-1181, doi:10.1007/s11431-017-9314-6, 2018a.

Zou, H., et al.: Imaging energetic electron spectrometer onboard a Chinese navigation satellite in the inclined GEO orbit, Sci. China Tech. Sci., 61, 1845-1865, 2018b.

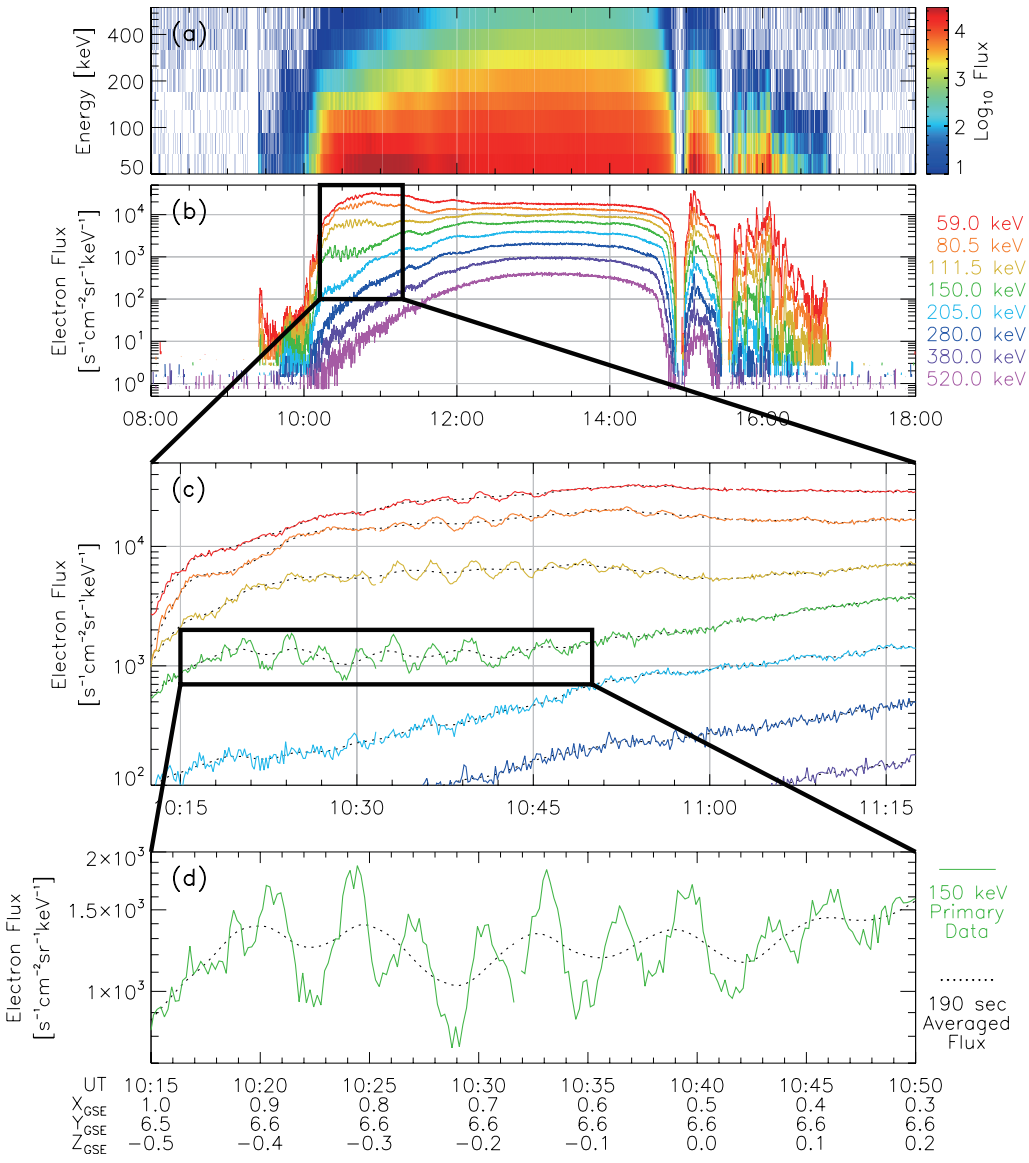

Figure 1. Overview of the electron flux observed by BD-IES. $(a)(b)$ Spectrogram and series plot of the electron flux in a full pass of the spacecraft through the radiation belt on October 13, 2015. (c) Zoomed-in view of the electron flux oscillation. (d) Zoomed-in view of the multi-period electron flux modulation.

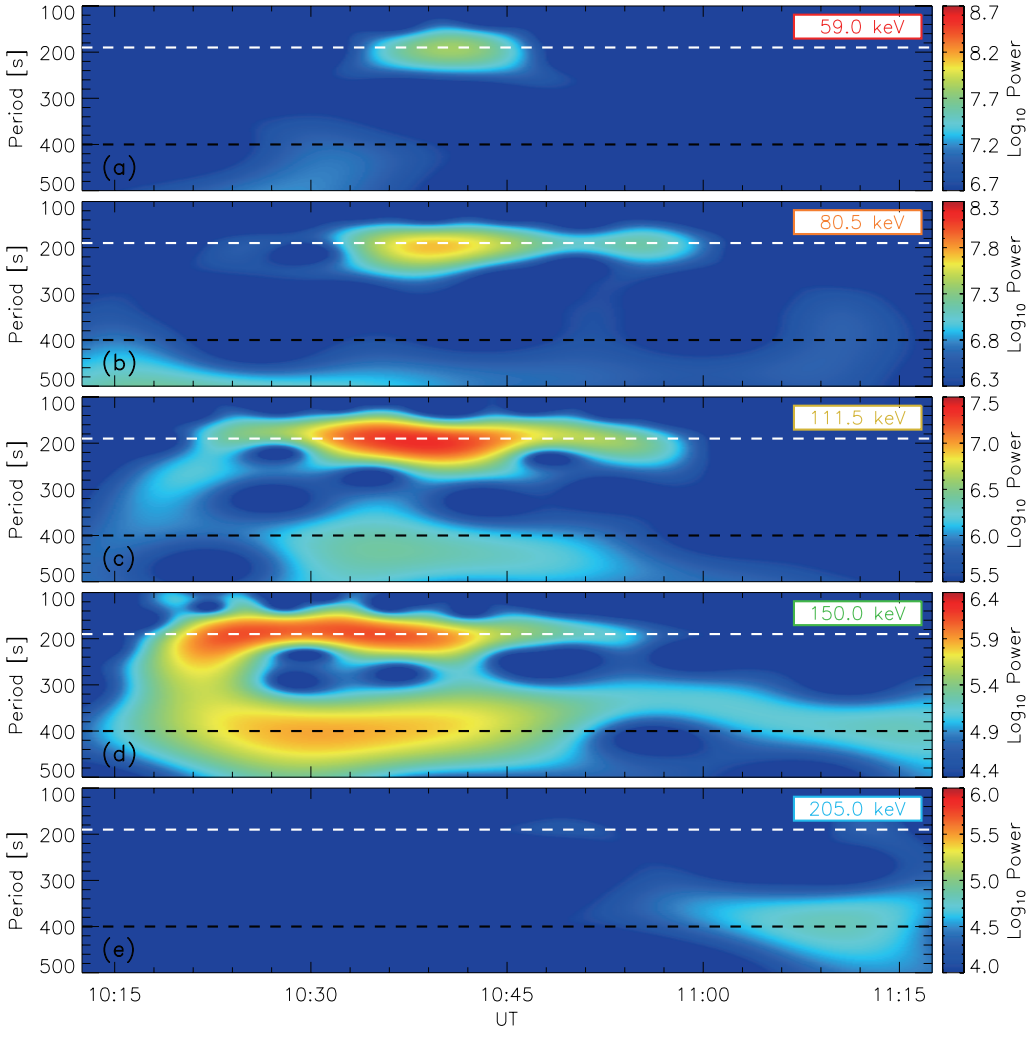

Figure 2. Wavelet analysis of the electron fluxes. (a)-(e) Wavelet power spectrograms of the electron fluxes from 59 keV to 205 keV. The white and black dashed lines mark 190 s and 400 s respectively.

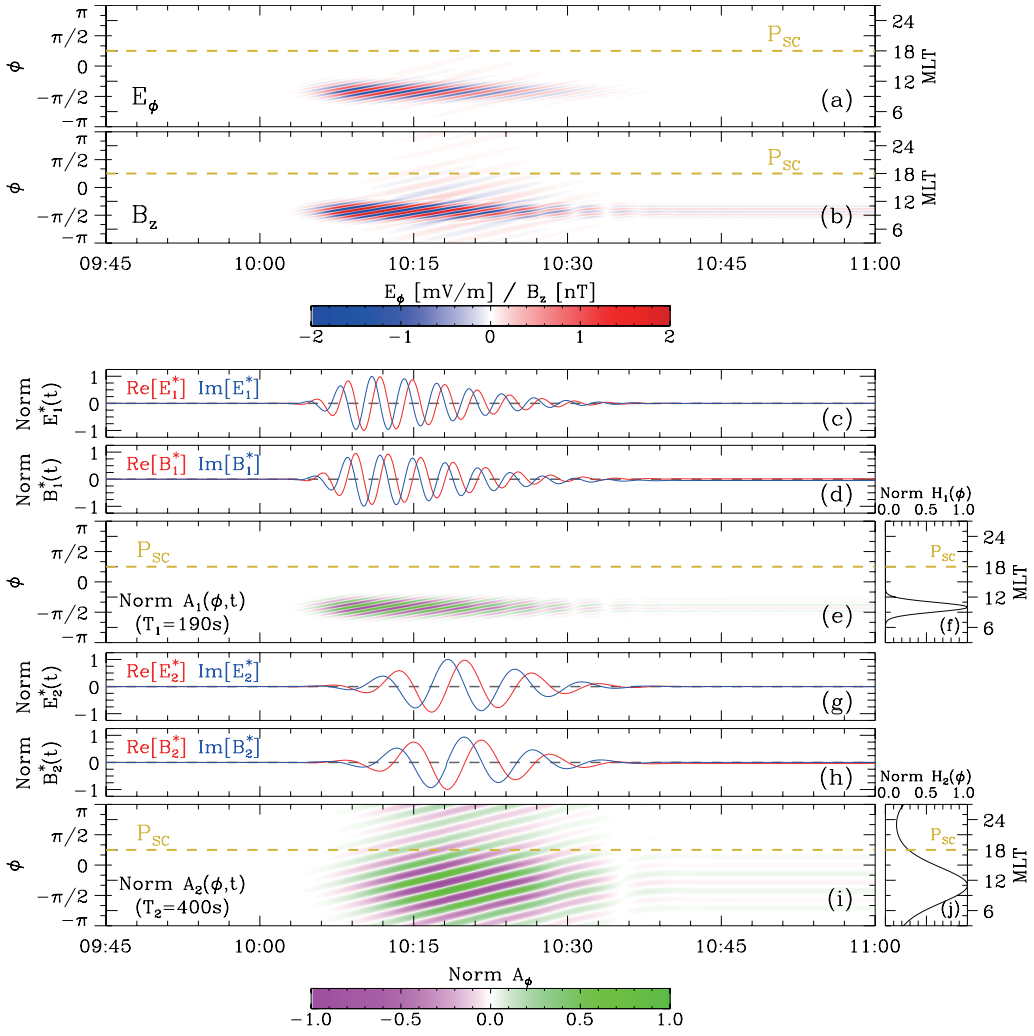

Figure 3. The modeled ULF electric field. $(a)(b)$ The modeled wave electric field and magnetic field as a function of UT and MLT. (c)-(j) The normalized azimuthal distribution and temporal evolution of each monochromatic wave. $\varphi = 0$ corresponds to $MLT = 15$. The horizontal dashed line marks the azimuthal location of the virtual spacecraft.

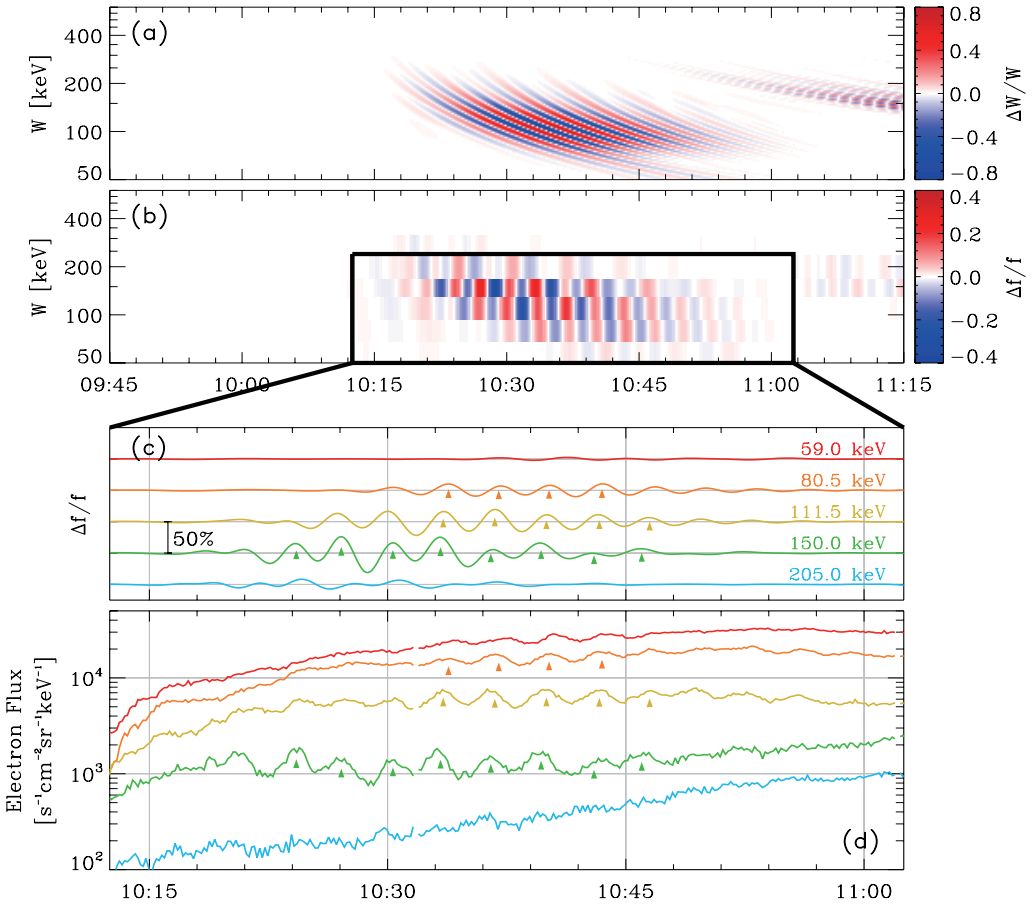

Figure 4. The modeled electron energy change and the corresponding residual flux. (a) The energy change of the electrons in the modeled ULF wave field. (b) The spectrogram of the modeled electron residual flux observed by the virtual spacecraft. (c) Zoomed-in view of the calculation result. (d) The electron flux observed by BD-IES. The triangles mark the modulation peaks.

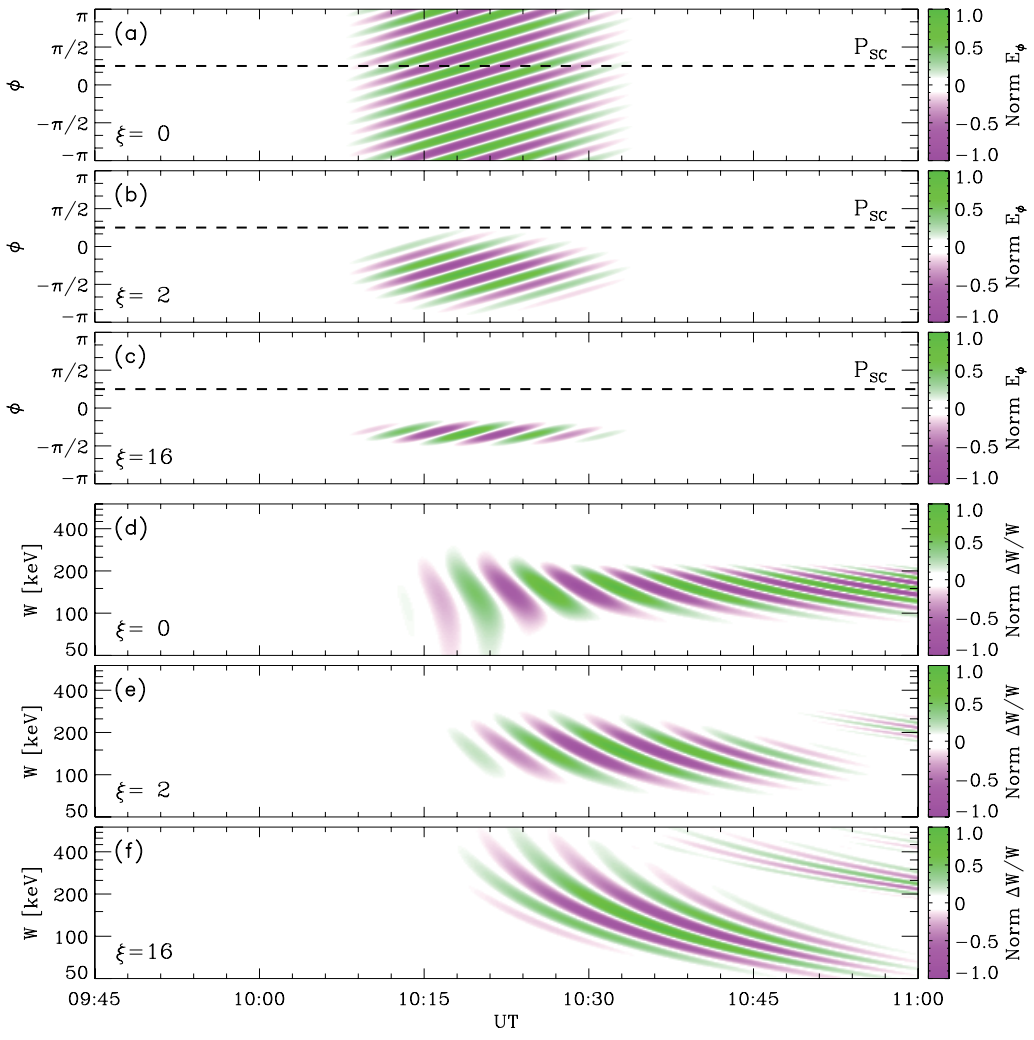

Figure 5. The width of electron flux modulation varied with the azimuthal distribution of the modeled ULF waves. (a)-(c) Modeled ULF waves of different spatial extents in the azimuthal direction. (d)-(f) The normalized electron energy gains from the corresponding ULF waves.